Marine Geology 477 (2024) 107386

Contents lists available at ScienceDirect

Marine Geology

journal homepage: www.elsevier.com/locate/margo

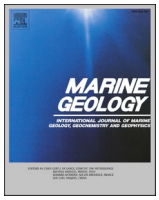

The Late Holocene evolution of the Adra Delta subaqueous system (Northern Alboran Sea): Seismic-stratigraphic and geomorphic evidence of millennial scale climatic and anthropic effects

P. Bárcenas [a,*], F.J. Lobo [b], L.M. Fernández-Salas [c], I. Mendes [d], N. López-González [a], J. Macías [e]

[a] CSIC–Instituto Español de Oceanografía, Centro Oceanográfico de Málaga, Puerto Pesquero s/n, 29640 Fuengirola, Málaga, Spain
[b] CSIC–Instituto Andaluz de Ciencias de la Tierra, Avenida de las Palmeras n° 4, 18100 Armilla, Spain
[c] CSIC–Instituto Español de Oceanografía, Centro Oceanográfico de Cádiz, Muelle de Levante s/n, 11006 Cádiz, Spain
[d] CIMA–Centro de Investigaçao Marinha e Ambiental, Rede de infraestrutura em Recursos Aquáticos (ARNET), Universidade do Algarve, 8005-139 Faro, Portugal
[e] Departamento de Análisis Matemático, Facultad de Ciencias, Universidad de Málaga, 29071 Málaga, Spain

ARTICLE INFO

Editor: Michele Rebesco

Keywords:
Mediterranean Sea
Deltaic system
Stratigraphic architecture
Climatic cycles
Anthropogenic interventions

ABSTRACT

The formation and development of a small Mediterranean deltaic system are investigated through a primary seismic stratigraphic interpretation of a high-resolution seismic profile network, combined with multiple bathymetric data (including multibeam bathymetric imagery) and collated with shallow sediment cores collected with a vibro-corer device.

The submarine delta of the Adra River is divided into a basal patchy seismic unit and five wedge-shaped younger seismic units that are related to the Holocene highstand stabilization. Limited age control indicates that the two uppermost seismic units are very recent, most likely related to a dearth of fluvial fluxes led by channel deviations and by sediment retention. The formation of the three older seismic units is correlated to three humid periods during the Middle Holocene, Late Holocene and Little Ice Age, under a general context of progressive aridification of southeastern Iberia.

The stacking patterns and spatial distribution of individual seismic units document a history of episodic progradation of successive prodeltaic lobes, with a long-term evolution mediated by climatically-induced changes in the river basin and more recent anthropogenic interventions. Overall, the subaqueous deltaic system registers the complete modification of a deltaic system that evolves from a fluvial-dominated delta to recent wave-dominated wedges. In between, the deltaic system exhibits a progressive asymmetric character, due to the instauration of Atlantic waters on the shelf and their subsequent eastward redistribution. The Adra deltaic system is proposed as an outstanding example of a small deltaic system that reacts almost immediately to the complex interaction between natural changes in the system and anthropogenic interventions in the drainage basin.

1. Introduction

Worldwide building of modern deltas was triggered during a restricted time interval (8.5–6.5 ka) due to a significant decrease in the rates of sea-level rise (Stanley and Warne, 1994). The short time spans involved in their development implied the stability of potential driving factors such as sea level and tectonics (Cattaneo et al., 2004). Instead, deltaic growth was controlled primarily by rapid climatically-driven fluctuations of river-borne sediments during periods of intensification of catastrophic river floods (Postma, 2001) and consequent increases in sedimentation rates, favouring rapid deltaic progradation (Anthony, 2014a), with variable sediment trapping efficiency according to delta size (Syvitski et al., 2022).

Sediment redistribution also constitutes a very important process governing deltaic growth, which inevitably gives rise to a dynamic equilibrium between longshore currents and river discharges. As a consequence, most deltaic systems tend to exhibit an asymmetric character (Anthony, 2015). In marine settings, the generation of sigmoidal wedges is influenced both by across- and along-shelf sediment transport (Liu et al., 2006, 2007). These processes include deltaic lobe switching, deflection of sediment plumes and longshore drift through marine oceanographic processes, as well as diverse coastal erosion processes

* Corresponding author.
E-mail address: patricia.barcenas@ieo.csic.es (P. Bárcenas).

https://doi.org/10.1016/j.margeo.2024.107386
Received 13 December 2023; Received in revised form 26 July 2024; Accepted 22 August 2024
Available online 30 August 2024

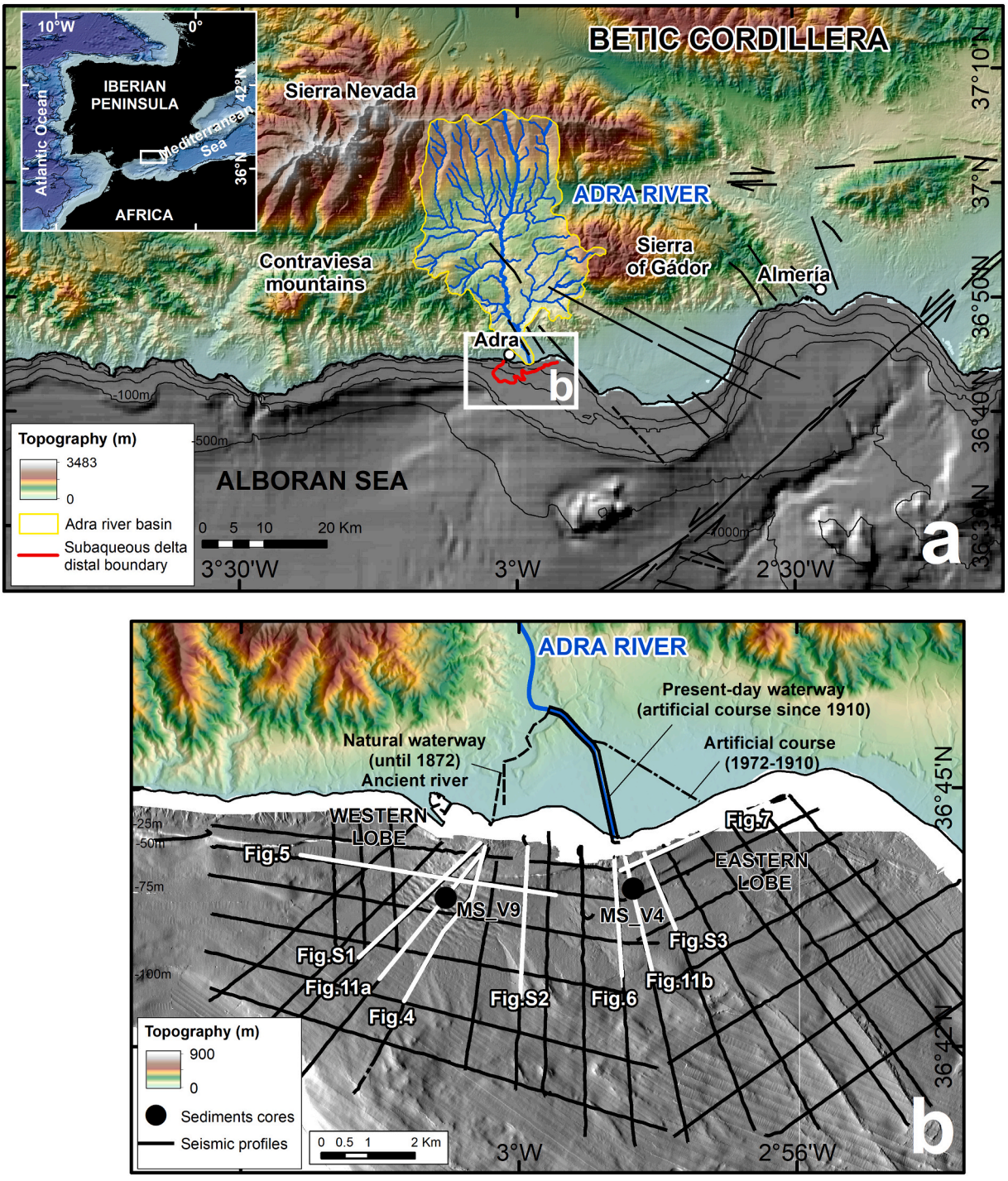

Fig. 1. Study area and location of seismic lines and core samples. Bathymetric data extracted from the ETOPO database are also shown. a) Offshore study area and inland topography derived from the DTM of the "Junta de Andalucía". A 60 m resolution hill-shaded bathymetric grid depicts the submarine physiography of the Alboran Sea. Major fault systems (black lines) are derived from Moreno et al. (2016). b) Seismic profiles and sediment cores obtained during the MOSAICO0908 survey. The shelf physiography is depicted by a 5 m resolution hill-shaded bathymetric grid acquired during the MOSAICO0509 survey. Two major deltaic deposits are recognized in the submarine deltaic environment: western and eastern deltaic lobes (see additional description in paragraph 2.3).

(Liu et al., 2004; Korus and Fielding, 2015). The lateral variability of such processes may affect the dispersal system, leading to contrasting geomorphic responses (e.g., Liu et al., 2006; Cattaneo et al., 2007; Xue et al., 2010), although most subaqueous deltas also tend to exhibit asymmetric patterns (Korus and Fielding, 2015).

The alternance of depositional versus erosional events also influences the internal architecture of subaqueous deltas, producing constructional blocks which stack vertically and/or horizontally (e.g., Neill and Allison, 2005; Cattaneo et al., 2003) and which may be interrupted by erosional phases involving shoreline retreat and marine erosion (Flocks et al., 2006). This is particularly relevant in the last few centuries, when the increased influence of human populations on fluvial catchments have profoundly affected the sedimentary balances in deltaic systems; in deltas affected by significant reductions of sediment supply, coastal erosion is a likely phenomenon (Besset et al., 2019).

The Mediterranean Sea is a privileged delta-forming environment,

due to the sediment supply conditions and redistribution of river-borne sediments by oceanographic processes. On the one hand, small rivers with marked seasonality constitute a major contributor of sediment supply to the Mediterranean, as they have very high sediment yields. In addition, narrow shelves and microtidal conditions favour the dominance of wave regimes along most Mediterranean coasts, which can be regarded as wave-dominated (Anthony, 2014b). Furthermore, a long-term history of human occupation and pressure on the drainage basins and by extension on their deltaic realms is recorded in these particularly sensitive environments. Major growth phases of the modern deltaic apparatus in the Mediterranean Sea are, in fact, strongly determined by intervals of enhanced anthropic pressure on the landscapes, as these interventions have modulated or counteracted natural processes (Maselli and Trincardi, 2013; Anthony, 2014b). The impact of anthropogenic perturbations (e.g., upstream dam construction, de- and re-forestation, dredging activities, etc.) on sediment budgets of deltaic systems has been overwhelming during the last two centuries (Anthony, 2014b), resulting in an enhanced influence of waves on the deltaic systems, and causing extensive erosion of deltaic shorelines (Anthony et al., 2014; Besset et al., 2017).

The general picture of Mediterranean-type deltaic evolution is biased towards the larger fluvio-deltaic systems, such as the Nile, Rhône, Ebro and Po, of great economic, societal and historic relevance (e.g., Díaz and Ercilla, 1993; Somoza et al., 1998; Stanley and Warne, 1998; Correggiari et al., 2005a, 2005b; Fanget et al., 2013, 2014; el Bastawesy et al., 2020; Trincardi et al., 2020) However, the record of climatic variations may be better preserved in the submarine portions of minor deltaic systems fed by small drainage basins (Postma, 2001). In addition, smaller deltas are more sensitive to marine hydrodynamics (Anthony, 2015) and therefore they can be used to reconstruct the influence of shallow-water circulation. The Adra River deltaic system, in the northern Alboran Sea (Western Mediterranean Basin) at the southeastern coast of the Iberian Margin (Fig. 1), is a relevant example. During the evolution of this deltaic system some drastic changes have occurred as a consequence of both natural processes and anthropogenic actions. Hence, the natural variations of sediment supply and the source-to-shelf transport processes recorded in the clinoforms may be enhanced by the steep physiography of the area and the extreme torrential behavior of the rivers (Liquete et al., 2005). On the other hand, man-driven fluvial regulations have also induced important changes in the area (Jabaloy-Sánchez et al., 2010). Considering all the evidence at hand, the aim of our study is to reconstruct the main evolutionary patterns for the Adra River deltaic system by interpreting a broad database comprising bathymetric data with different resolutions, high-resolution seismic profiles and sediment cores. Specifically, the high-resolution seismic dataset allows distinguishing the detailed internal architecture of deltaic deposition in the area, which could be correlated with century-scale climatic events. Eventually, the influence of climatically-induced sediment supply and paleoceanographic changes and more recent anthropic actions were retraced.

2. Regional setting

2.1. Geological setting

The southeastern Iberian margin hosts the convergent boundary between the European and African plates. In this margin, the main tectonic structure is the Eastern Betic Shear Zone, which has been active during the Pliocene and Quaternary (Moreno et al., 2016). The Adra River drainage basin is located north of this shear zone (Fig. 1a). The Adra River deltaic system is crossed by WNW–ESE to NNW–SSE trending oblique-normal faults perpendicular to the Eastern Betic Shear Zone (Moreno et al., 2016), that resulted from orthogonal extension to the main NNW–SSE compression (Galindo-Zaldívar et al., 2019). The convergent regime determined tectonic uplift at low rates (i.e., 7 cm/ka) during the Late Pleistocene along the southeastern coast of Iberia (Zazo et al., 1993; Galve et al., 2020).

The Adra River drainage basin extends along the central part of the Sierra Nevada. Laterally, it is confined by the Gádor and Contraviesa sierras (Fig. 1a). The basin mostly extends over metamorphic rocks of Palaeozoic to Triassic age, composing the Internal Zone of the Betic Cordillera (Carvajal and Sanz de Galdeano, 2008).

2.2. The Adra River drainage basin area

The Adra River basin covers 750.7 km^2 and reaches a maximum height of 2682 m. The Adra River has a permanent flow during the year, with a mean water discharge of 1 $m^3\ s^{-1}$. The mean sediment load and yield have been estimated at 4.8 kg s^{-1} and more than 200 t $km^{-2}\ yr^{-1}$, respectively (Liquete et al., 2005).

In the nearby Sierra de Gádor, analysis of vegetation distribution patterns indicates a mid-Holocene wet and warm phase (Gil-Romera et al., 2010). An overall aridification trend since the last ca. 6 ka (Carrión et al., 2003) has been punctuated by several humid periods recorded by changes in vegetation, fires and lake sedimentation in the nearby Sierra Nevada (Jiménez-Moreno et al., 2013; Ramos-Román et al., 2016).

More recently, three periods entailing catastrophic floods have been reported in the past five centuries along the Iberian Mediterranean coast (Barriendos Vallve and Martin-Vide, 1998). Human modification of the river basin during the last two centuries includes intensive mining, initiated in the early 19th century and accompanied by increased firing activity (Gil-Romera et al., 2010). The terminal river course underwent two deviations to prevent damage from flooding in the deltaic plain: the first from 1862 to 1872 and the second in 1910, when the Adra Harbour was built (Cuéllar Villar, 2006). The most recent intervention in the river basin was the construction of the Beninar Dam, completed in 1983 (Jabaloy-Sánchez et al., 2010).

2.3. The Adra subaqueous delta

In the Adra deltaic system, previous studies have focused on the deltaic coastline, which exhibits three evolutionary stages conditioned by the interaction of natural and anthropogenic influences (Jabaloy-Sánchez et al., 2010). The first phase extended from 4000 BCE to 1872 CE and involved the generation of an asymmetrical triangular delta, mostly as the result of a natural evolutionary process (Jabaloy-Sánchez et al., 2010). The second phase occurred between 1873 and 1972, influenced by changes of river channel locations that promoted the erosion of the older deltaic lobe and the construction of a new lobe off the artificial channel, under conditions of decreased sediment supply. The third phase, since 1972, is characterized by widespread coastline erosion due to the influence of the Beninar Dam (Jabaloy-Sánchez et al., 2010).

Offshore, the influence of the Adra River deltaic sedimentation is restricted to the inner and middle shelf. Two major deltaic protuberances are recognized in the submarine deltaic environment (Jabaloy-Sánchez et al., 2010; Mendes et al., 2015). The western deltaic lobe is found off the natural river waterway, extending 2 km in a southwest direction. This lobe is shaped by seafloor undulations likely reflecting the effect of fluvially-derived flows (Bárcenas et al., 2009). The surface sediments are composed of proximal sandy gravels and distal muddy sands. The eastern deltaic lobe is composed by elongated sandy wedges (Bárcenas et al., 2011). Two sediment cores retrieved from the western (MS_V9) and eastern (MS_V4) lobes of the subaqueous deltaic deposit, reflects the natural climatic variability and anthropogenic impacts occurred in this area since ca. 1660 CE (Mendes et al., 2015). Periods of increased coarse-grained sediments were related with major rainfall or flooding events, whereas periods of increased percentages of fine-grained sediments were linked to periods of low rainfall or dry conditions. The human interventions on the river basin after 1872 CE, with the deviation of the main river channel to the east, led to a

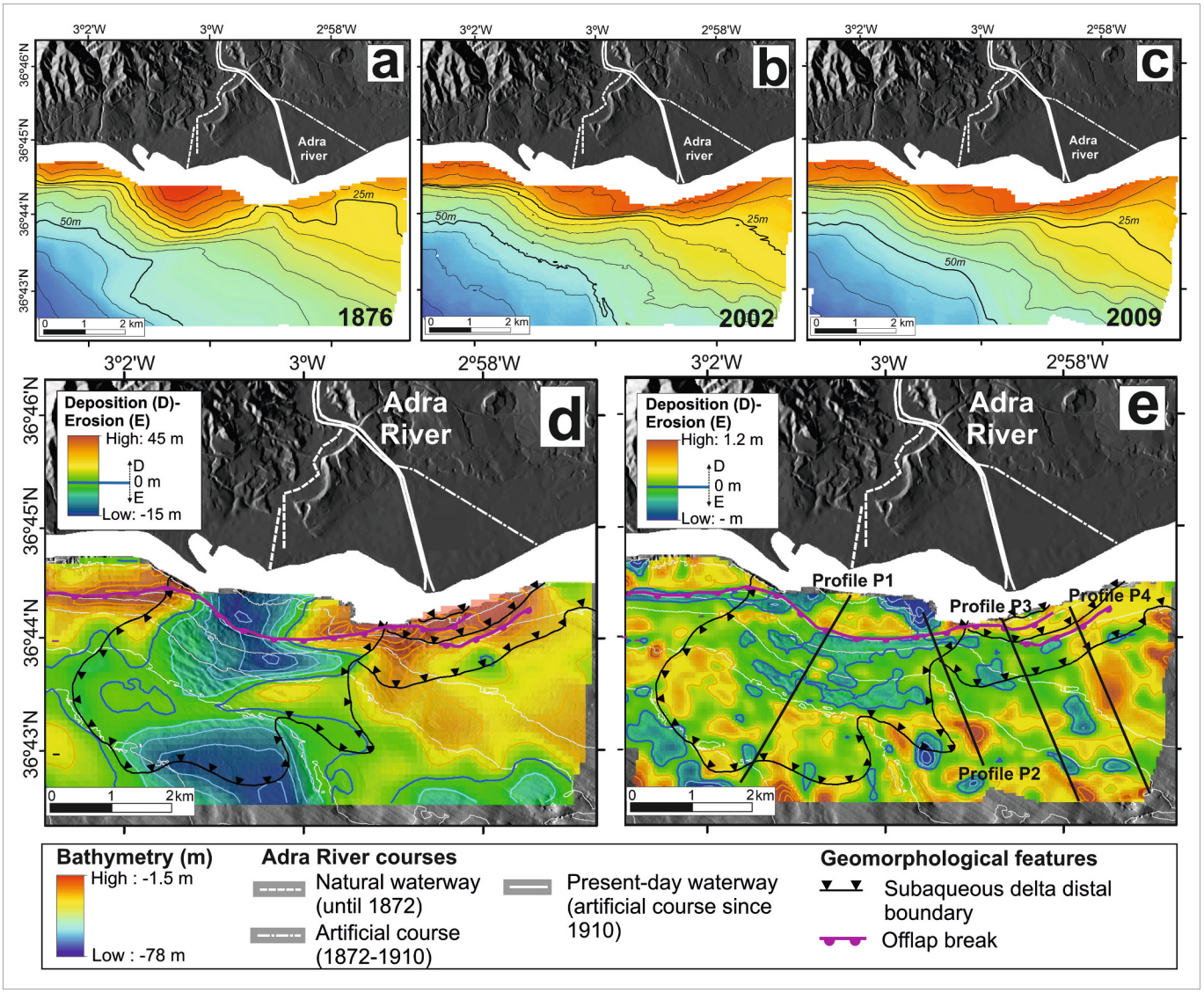

Fig. 2. Bathymetric changes in the area of the Adra subaqueous delta evidenced by different temporal maps. a) 1876 bathymetric map; b) 2002 bathymetric map; c) 2009 bathymetric map; d) depositional-erosional areas for the period 1876–2009; e) depositional-erosional areas for the period 2002–2009. The deposition-erosion scale represents the height of a sediment column of with a 1 m^2 base. Profiles P1-P4 are shown in Fig. 3.

drastic reduction of the sediment exported to the western delta lobe. The following human interventions on the Adra river basin led to a drastic reduction of the sediment exported to the shelf (Mendes et al., 2015).

2.4. Oceanographic setting and relative sea-level changes

Longshore currents and littoral drift are favoured in this E-W oriented coast, and exhibit a main component of sediment transport from west to east (Goy et al., 2003). To the east off the Spanish coast in the Alboran Sea, harmonic analyses of current meter data revealed tidal amplitudes reaching 6–9 cm/s (García Lafuente and Lucaya, 1994). In areas of the Almeria coast, lower values of tidal currents between 2 and 4 cm/s are observed (Albérola et al., 1995; Poulain et al., 2018).

Regional shallow-water circulation is influenced by the entry of Surface Atlantic Water (SAW) through the Strait of Gibraltar. The inflow is directed eastward along-margin, where the northern Alboran Sea is shallower than 200 m (e.g., Sayol et al., 2013; Oguz et al., 2016). However, shelf current patterns parallel to the regional bathymetric contours exhibit temporal reversals from westerlies to easterlies (Bárcenas et al., 2011).

Records of Holocene sea levels have been provided along several coastal sectors of the northern Alboran Sea (Lario et al., 1999; Goy et al., 2003). Three millennial-scale sea-level fluctuations of sub-metric amplitude occurred after a relative sea level maximum at about 5.4 cal ka. These cycles show prolonged sea level drops, the minimum sea levels apparently connected with periods of extended aridity and increased intrusion of SAW (Goy et al., 2003).

3. Materials and methods

3.1. Bathymetric data

We used bathymetric data and derived digital elevation models (DEMs) from three different years : 1876, 2002 and 2009 (Fig. 2). Multibeam bathymetric data used for the 2002 and 2009 DEMs were acquired with two different multibeam echo sounders (EM3000D and EM3002D) in two different oceanographic surveys performed by the Spanish Oceanographic Institute. In the ESPACE02 survey carried out between April and September 2002, the multibeam data offered 100 % coverage, from 9 to 10 m to 160 m water depths. The EM3000D

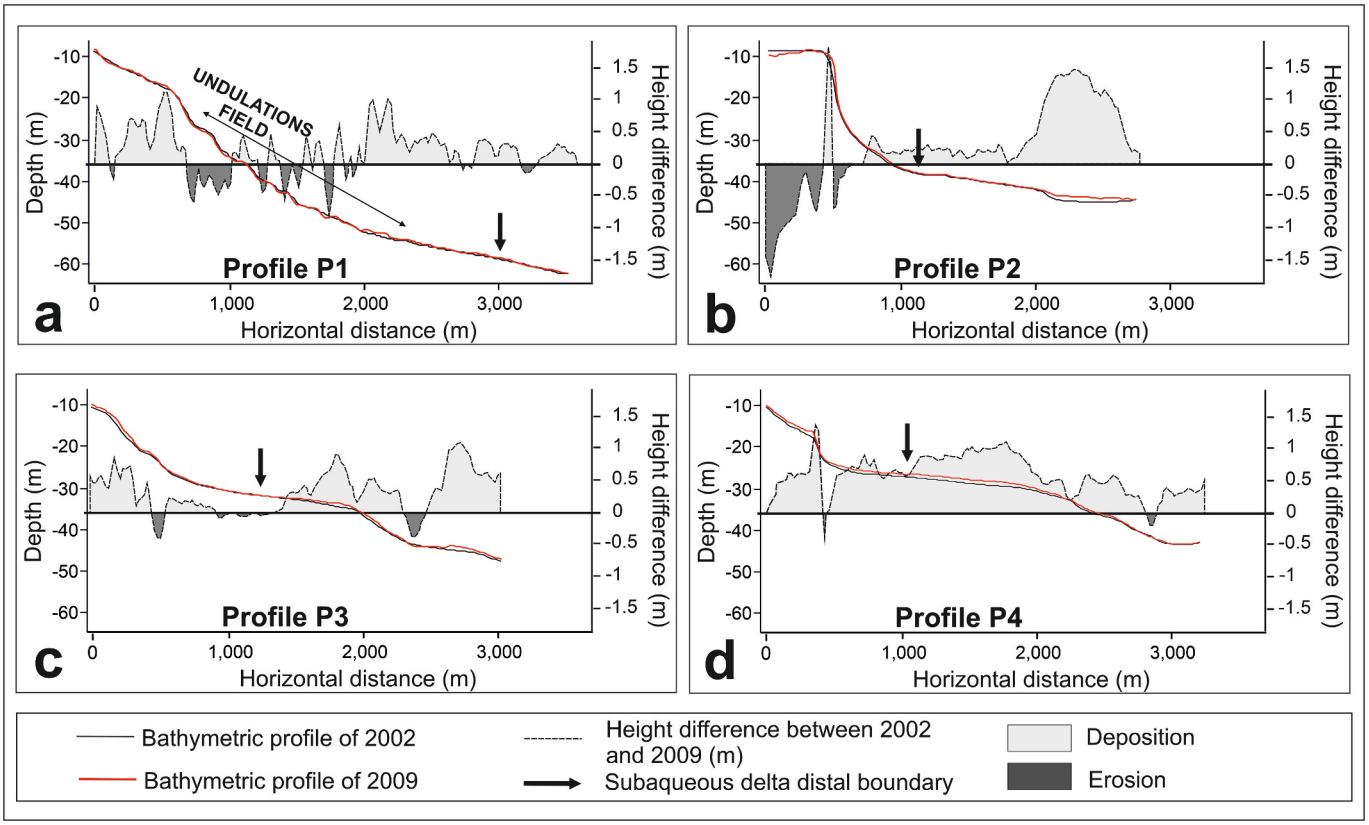

Fig. 3. Height difference along bathymetric profiles relative to the 2002 and 2009 bathymetries (location of profiles in Fig. 2). The height of differential erosion/deposition is also reported (dashed line).

multibeam echosounder emits 254 beams with a swath width up to five times the water depth. The motion sensor Seatex Seapath 200 provided real-time pitch, heave and roll corrections. In the MOSAICO0509 survey executed between May 2–82,009 data were acquired from 7 to 82.5 m water depths. The EM3002D multibeam echosounder provided 508 beams of depth information. Neptune™ and Caraibes™ software were used to process raw multibeam data, and 5 m resolution grids were generated. From the processed data, digital terrain models (DTM) were generated using ArcGIS™ software. The interpolation method was gridding based on a Gaussian weight averaging scheme. The cell size chosen was 5 × 5 m. Subsequently, both bathymetries were smoothed to 50 m resolution for comparison with the bathymetry of 1876.

Historical bathymetric data were extracted from the most modern edition of the nautical chart of Montojo y Salcedo (1876). This historical map was analyzed using a Geographic Information System (GIS); the map was scanned and georeferenced using 29 control points regularly spaced through the UTM grid of the map, having applied a third order polynomial transformation. Once the raster dataset was adjusted to the coordinate system, the residual errors related to the difference in location of control points in the historical map and their real locations were computed. The RMS (root mean square) error obtained was 237.3 m. A digital elevation model with a 50 m horizontal resolution was generated (additional details contained in Jabaloy-Sánchez et al., 2010).

Volumetric changes defining depositional and erosional areas in the submarine delta were approximated with 50 m resolution grids using ArcGIS™ at longer (i.e., secular) and shorter (i.e., interannual) timescales (Fig. 2d and e). Based on these bathymetric differences performed with the cut and fill tool of the Spatial Analyst module of the ArcGIS™ typically used to calculate volume changes between two surfaces, sediment yield rates in the catchment were estimated, using an average sediment density of 1.85 t m^{-3}, according to inland gravimetric modeling and offshore drill modeling (Martínez-García and Soto, 2006; Duque et al., 2008). The estimates of volume changes can be regarded as rough approximations, as they are limited by the resolution of the initial grids and by location errors of the historical bathymetric data.

3.2. High-resolution seismic profiles

A Uniboom seismic source was used during the MOSAICO0908 cruise for the acquisition of 254 km of high-resolution seismic profiles off the Adra River and adjacent zones (Fig. 1b). The seismic profiles are laterally spaced about 1 km and their orientation is normal or parallel to the coast. The pulse energy was 175 J, and the trigger interval was 400 ms. The recording length was 250 ms, and the seismic data were recorded in SEG-Y format using SonarWiz™ software. Data processing included gains, 0.5–2 kHz bandpass and swell filters.

A conventional seismic stratigraphy interpretation was made, by means of Kingdom™ software. Several seismic horizons showing high amplitude and lateral continuity were traced along the deltaic deposits, enabling the distinction of seismic units with specific seismic facies which constitute the building blocks of subaqueous deltaic deposition in the study area, as documented in comparable settings (e.g., Fernández-Salas et al., 2003; Casalbore et al., 2022).

3.3. Chronostratigraphic framework

The chronostratigraphic framework of the studied deposits is based on the calibration of the seismic stratigraphic interpretation with limited ages derived from sediment cores. For the purposes of this study, two sediment cores previously analyzed by Mendes et al. (2015) were selected. Sediment cores MS_V9, 187 cm long and retrieved in the western lobe at 41.5 m water depth and MS_V4, 154 cm long and extracted from the eastern lobe at 26.5 m water depth (Fig. 1b). Core MS_V9 contained laminated sandy silts, with the sand fraction prevalent

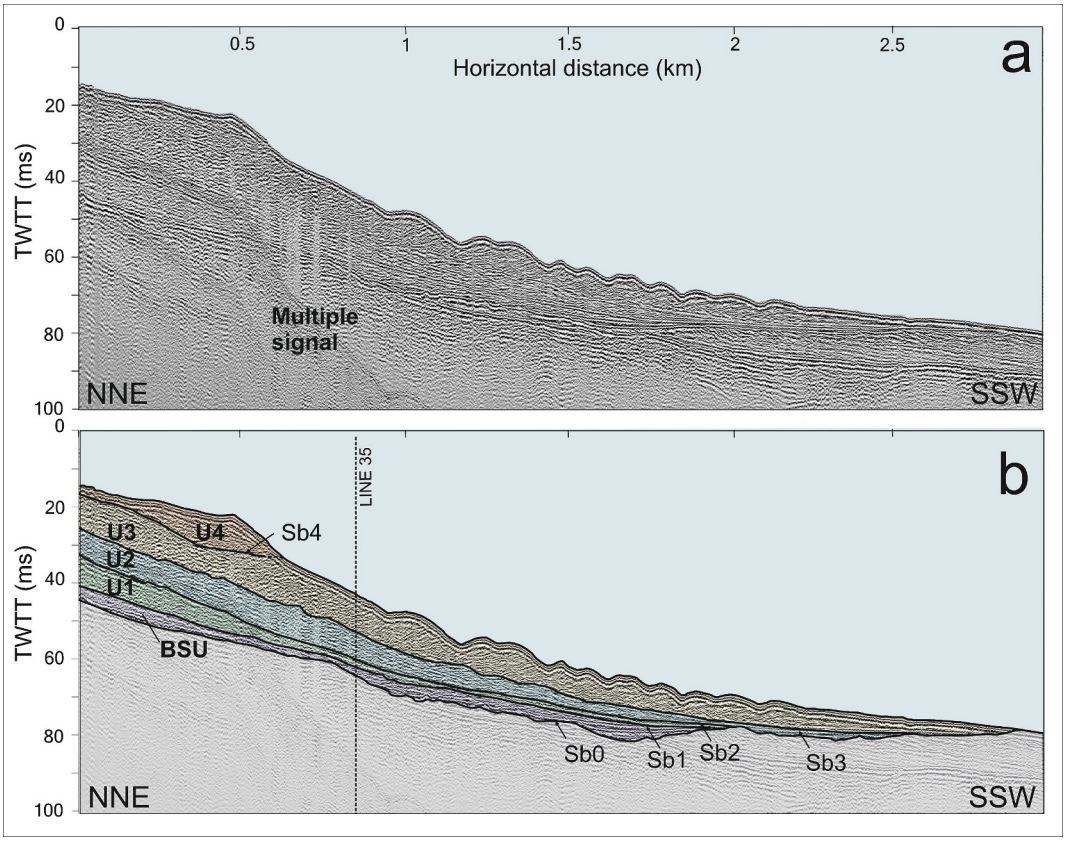

Fig. 4. Cross-shelf stratigraphic architecture of the western lobe of the Adra subaqueous delta. a) Uninterpreted high-resolution Uniboom seismic profile (TWTT: Two-way travel time in milliseconds); b) Interpreted seismic profile, including seismic units (BSU, U1, U2, U3 and U4) and bounding unconformities (Sb0 to Sb4). Location of seismic profile is indicated in Fig. 1b.

in the upper 10 cm. Radiocarbon dating from sediment samples from the base of MS_V9 (182–183 cm depth) indicated a conventional age of 240 ± 30 yr BP, corresponding to a median probability of ca. 290 cal yr BP (1663 CE), and an additional age of 210 ± 30 yr BP, with median probability calibrated age of ca. 180 cal yr BP (1776 CE) from sediment at 50–51 cm from the top of the core. Two sedimentary intervals were identified in core MS_V4. The lower interval, from the core base to ca. 30 cm depth, contains fine-grained sediments, while the upper interval, representing the top 30 cm, contains more than 90 % of sand. Dating at the base of core MS_V4 (152–153 cm depth) indicates a conventional radiocarbon age of 170 ± 30 yr BP, corresponding to a median probability calibrated age of ca. 180 cal yr BP (1774 CE) (Mendes et al., 2015).

The extrapolation of sedimentation rates inferred from sediment core MS_V9 enabled to provide age constraints for the younger deltaic units. Additionally, the change in stratigraphic architecture at the base of the succession was interpreted in terms of sequence stratigraphy, providing a basal age estimation.

As no age data are available for the intermediate deltaic deposits, we propose a tentative correlation and timing of events based on: (1) the spatial distribution of seismic units and their possible relationship with different river channels; (2) the comparison of the observed architectures with well-known climatic changes that have occurred in the southeastern Iberian Peninsula throughout the Holocene; and (3) the comparison with other deltaic evolutionary patterns in the Mediterranean. This approach should be considered as approximative, and should be improved in the future by collecting material for age data in each of the units composing the entire deltaic succession.

4. Results

4.1. Estimates of changes in sediment volumes

Changes in sediment volumes and depositional-erosional patterns in the study area were estimated through the comparison of bathymetric data collected in different years (Figs. 2a, b and c); on a secular scale, between 1876 and 2009 (Fig. 2d) and on an interannual scale, between 2002 and 2009 (Fig. 2e). The overall bathymetric characterization and features of the submarine deltaic deposits inthe study area are derived from Jabaloy-Sánchez et al. (2010) and Mendes et al. (2015).

A comparison of 1876 and 2009 bathymetric data reveals the occurrence of two main sediment accumulation areas: west of the western lobe, and over the entire eastern lobe (Fig. 2d). A sediment volume gain of 4.5×10^7 m^3 is estimated, equivalent to an accumulation rate of $\sim 3.3 \times 10^5$ m^3 yr^{-1}. The widespread erosion of the western lobe of the deltaic system is outstanding (Fig. 2d). The total volume of sediment eroded is $\sim 1.5 \times 10^7$ m^3, which comes to an annual rate of 1.1×10^5 m^3 yr^{-1}.

Between 2002 and 2009, sediment accumulation in the eastern lobe is again observed (Fig. 2e). The total sediment accumulation is 0.1×10^7 m^3, with an accumulation rate of $\sim 1.6 \times 10^5$ m^3 yr^{-1}. During this recent interval, there is still neat erosion in the western lobe (Fig. 2e), with a total sediment volume loss of $\sim 0.9 \times 10^7$ m^3 and an estimated erosion rate of $\sim 1.3 \times 10^5$ m^3 yr^{-1}.

Several cross-shelf profiles allow us to improve the description of the small-scale deposition-erosion pattern of the subaqueous deltaic deposits in the area (Fig. 3). These profiles show that overall bathymetric relief decreases in the western lobe, along the foreset undulation field (Fig. 3a) and over the side areas of the topset (Fig. 3b). The eastern lobe has mostly been a depositional area, with some erosional spots seaward

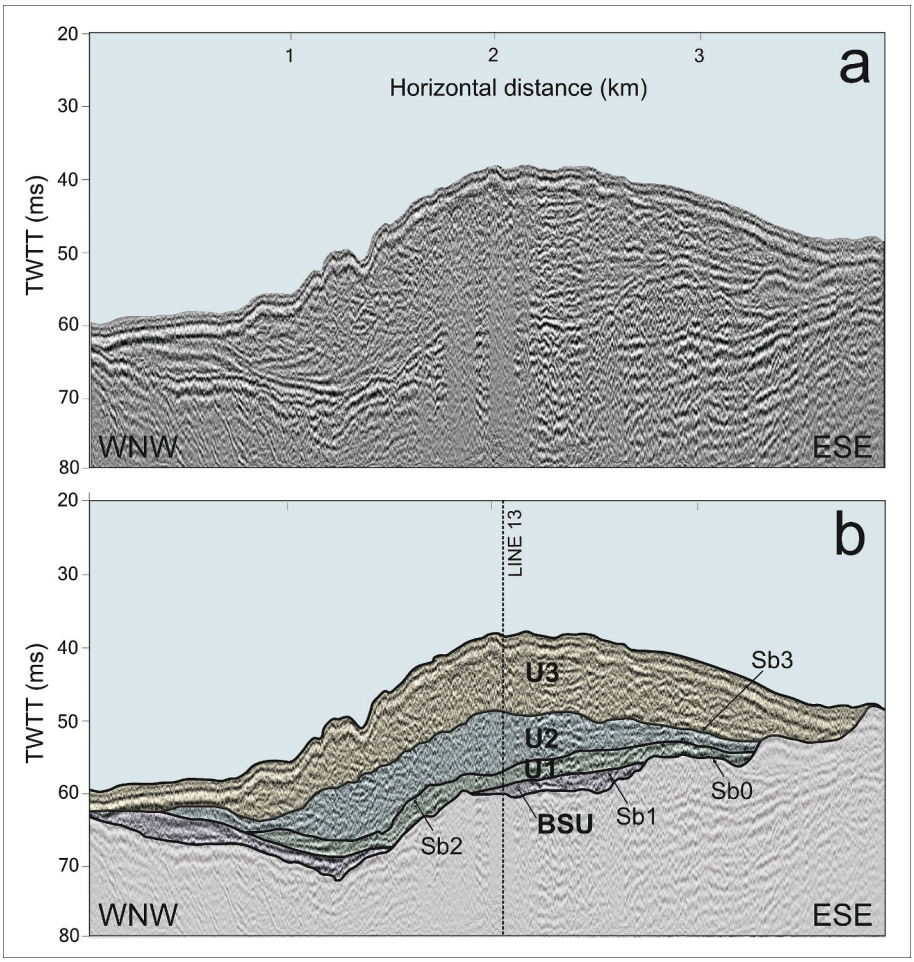

Fig. 5. Along-shelf stratigraphic architecture of the western lobe of the Adra subaqueous delta system. a) Uninterpreted high-resolution Uniboom seismic profile (TWTT: Two-way travel time in milliseconds); b) Interpreted seismic profile, including seismic units (BSU, U1, U2 and U3) and bounding unconformities (Sb0 to Sb3). Location of seismic profile is indicated in Fig. 1b.

of the inner wedges (Fig. 3c and d).

4.2. Seismic stratigraphic interpretation

The subaqueous delta off the Adra River comprises five main seismic units (U1 to U5) over a discontinuous Basal Seismic Unit (BSU) (Figs. 4 and 5). The studied seismic units are separated by primary seismic horizons used as seismic-stratigraphic boundaries (from older to younger named Sb0 to Sb5). The basal boundary Sb0 is a high-amplitude seismic horizon forming a regional unconformity interpreted as a polygenetic surface recording shelf subaerial exposure during the Last Glacial Maximum and subsequent reworking during the postglacial sea-level rise, in accordance with evidences from other deltaic deposits in this region, where equivalent post-last glacial unconformities have been defined (e.g., Ercilla and Alonso, 1996; Fernández-Salas et al., 2003; Lobo et al., 2006, 2015; Casalbore et al., 2022). The seismic facies and spatial distribution of seismic units allow the definition of two sectors differing in their overall geomorphology. The western sector is situated off the ancient river mouth location (until the end of the 19th century) (4, 5, S1 and S2), and the eastern sector is situated off the most recent river mouth positions (Figs. 6, 7 and S3), which shifted in accordance to river deviations, as described in the study area section.

4.2.1. Seismic units

The BSU is bounded at the bottom by a high-amplitude seismic horizon (Sb0) which locally exhibits rugged patterns, whereas its top boundary (Sb1) also exhibits local corrugations. High-amplitude and discontinuous concordant internal reflectors within the BSU exhibit local onlap terminations. In cross-sections, the unit exhibits a sheet-like geometry with lateral thickness changes due to the underlying irregularities (Figs. 4, 6, S1, S2 and S3).

Seismic unit U1 displays a parallel-oblique configuration with internal reflections attenuating and becoming more parallel seaward (Figs. 4, S1 and S2). Internal reflectors exhibit downlap terminations over the lower boundary (Sb1), whereas toplap to erosional truncation occurs atop (Sb2). The upper boundary (Sb2) exhibits a smooth topography off the ancient river mouth. The cross-section external morphology is wedge-shaped.

Seismic unit U2 exhibits distinctive seismic facies in both sectors, as the internal configuration is parallel-oblique in the western sector (Figs. 4, S1 and S2) and changes to tangential-oblique towards the eastern sector (Figs. 6 and S3). Reflection terminations are basal downlap to concordance and top erosional truncation to toplap. U2 is wedge-shaped in the west and bank-like shaped in the east (Figs. 4, 6 and S3).

Seismic unit U3 buries the underlying units (U1 and U2) and is exposed in the present-day seafloor over most of the western sector (Figs. 4,5 S1 and S2) and partially in the eastern sector (Fig. 7). U3 has a highly reflective acoustic response and also shows differences in the internal configuration in both sectors. In the west the internal configuration is chaotic, with frequently changing reflection geometry, from landward inclined to parallel-oblique in the distal areas (Figs. 4, S1 and S2). In the east the internal configuration is tangential-oblique (Fig. S1). Downlap terminations are observed over the lower boundary, whereas

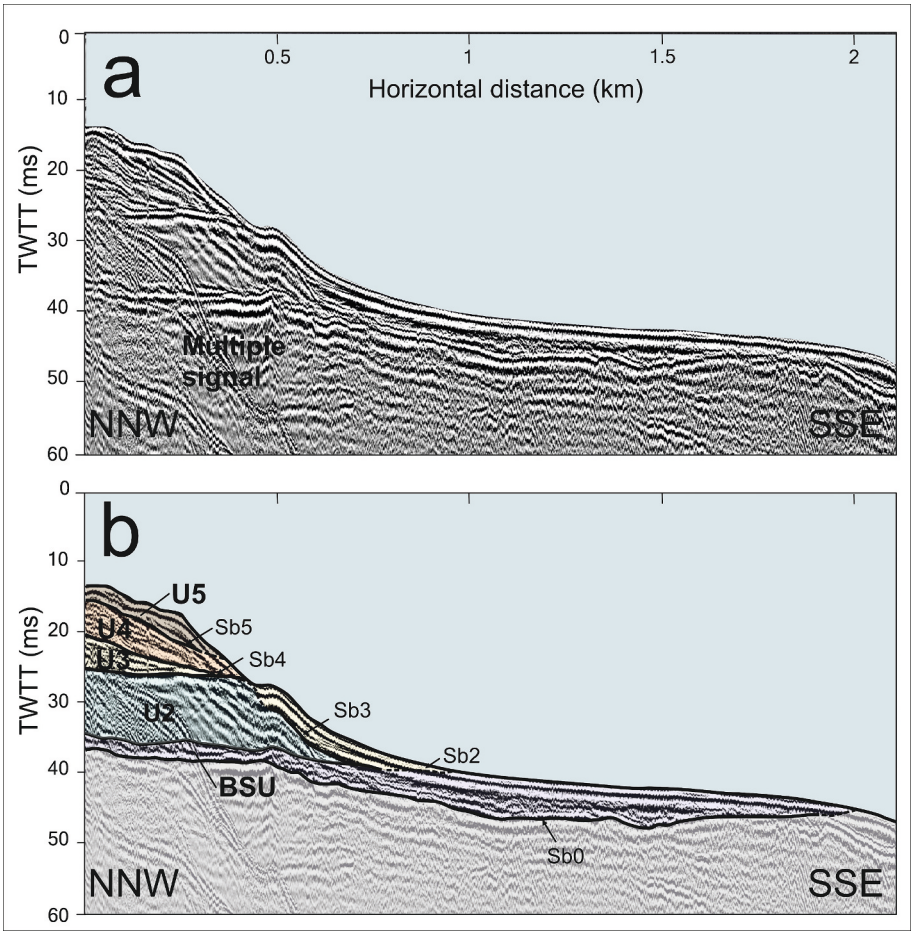

Fig. 6. Cross-shelf stratigraphic architecture of the eastern lobe of the Adra subaqueous delta system, off the present-day river mouth. a) Uninterpreted high-resolution Uniboom seismic profile (TWTT: Two-way travel time in milliseconds); b) Interpreted seismic profile, including seismic units (BSU, U2, U3, U4 and U5) and bounding unconformities (Sb0, Sb2, Sb3, Sb4 and Sb5). Location of seismic profile is indicated in Fig. 1b.

the upper boundary tends to exhibit proximal erosional truncation and distal toplap. This upper boundary exhibits a well-marked undulatory pattern in the areas where U3 is exposed at the seafloor (Figs. 4, S1 and S2). The U3 is wedge-shaped in the western sector, changing to bank-like off the present-day river mouth (Figs. 4, 6 and S1 to S3).

Seismic unit U4 shows a tangential-oblique configuration evolving to parallel-oblique eastwards. Internal reflectors downlap the lower boundary. It shows toplap with the upper boundary except off the present-day river mouth, where erosional truncation occurs. It exhibits a bank external shape in cross-sections (Figs. 4, 6 and S1 to S3).

Seismic unit U5 is the youngest unit, displaying a tangential-oblique configuration. The unit exhibits basal downlap and toplap terminations in the upper boundary that represent the present-day seafloor. U5 displays a bank external shape (Figs. 6, 7 and S3).

4.2.2. *Spatial distribution of seismic units*

The spatial distribution of the subaqueous deltaic deposits as a whole shows maximum thickness in the shallowest-water areas, with a gradual decrease to the south and to the east (Fig. 8). Three main depocentres are indicated as D1-D3 and show sediment thickness values > 20 ms (Fig. 9). D1 is an EN*E*-WSW depocenter of 33 ms maximum thickness located between the natural and the present-day waterways at 10.5 m water depth. D2 is a sub-circular depocenter, with 30.7 ms of maximum thickness, and is located off the ancient river mouth at 14 m water depth. A third NE-SW oriented depocenter (D3) with lower thickness (< 23 ms) is located on the present-day waterway mouth at 8.5 m water depth (Fig. 9).

The regional distribution of the BSU tends to parallel the coastline, extending seaward 3 km in front of the present-day river course (Fig. 10a). The sediment thickness ranges between 0 and 7.7 ms, with an average value of 2.3 ms and four main depocenters (Fig. 10a). A SE-NW oriented depocenter >6 ms thick occurs off the ancient river mouth. Slightly to the east, an E-W oriented depocenter with a maximum thickness higher than 6 ms is found. In front of the active waterway mouth, a depocenter with a maximum thickness ~ 6 ms and SE-NW orientation is observed. The last depocenter occurs between the two artificial courses of the river Adra, showing a maximum thickness of 6.4 ms and a SE-NW orientation (Fig. 10a).

U1 shows the maximum development off the ancient river mouth extending 3 km seaward, and it extends laterally less than 4 km. The maximum sediment thickness is 10.8 ms, with a mean value of 2.1 ms that decreases towards the south and southeast (Fig. 10b). The main E-W oriented lobate depocenter is located between the present-day waterway and the ancient river mouths.

U2 exhibits a wider distribution than U1. In the western sector off the ancient river mouth, this unit extends 1.8 km seaward with an overall lobate shape. This seismic unit parallels the coastline with an elongated shape in the eastern sector. The unit extends laterally for more than 9 km (Fig. 10c). U2 displays an average thickness of 4.3 ms. Two major depocenters are observed —one located off the ancient river mouth, with maximum thickness values of 7.9 ms and NE-SW orientation, and another ENE-WSW elongated depocenter located in the east showing a maximum thickness of 13.2 ms (Fig. 10c).

U3 extends laterally over 9 km along the shelf, being >4 km wide in

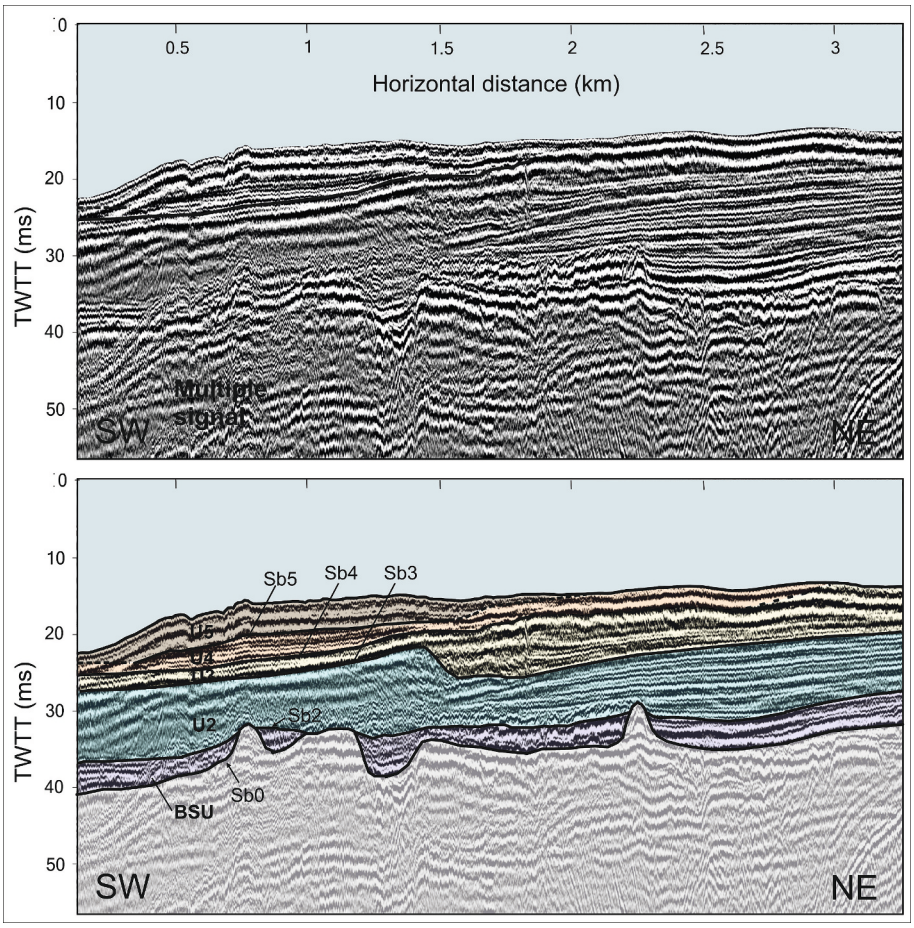

Fig. 7. Along-shelf stratigraphic architecture of the eastern lobe of the Adra subaqueous delta system, over the topset segment. a) Uninterpreted high-resolution Uniboom seismic profile (TWTT: Two-way travel time in milliseconds); b) Interpreted seismic profile, including seismic units (BSU, U2, U3, U4 and U5) and bounding unconformities (Sb0, Sb2, Sb3, Sb4 and Sb5). Location of seismic profile is indicated in Fig. 1b.

the western sector and 1.7 km wide in the eastern sector (Fig. 10d). It displays a maximum thickness of 12.7 ms with an average value of 3.8 ms, and a lateral distribution similar to U2 (Fig. 10d). However, in this case the maximum thickness values are located off the ancient river mouth, forming a main NE-SW depocenter. Off the artificial river courses, minor depocenters with thickness < 8 ms and ENE-WSW orientation are identified (Fig. 10d).

The spatial distribution of U4 is parallel to the coastline, forming an E-W elongated depocenter extending 7 km laterally and less than 2 km across the shelf (Fig. 10e). U4 shows the highest sediment thickness (16.7 ms) between the ancient and active waterways, displaying an E-W orientation (Fig. 10e).

U5 exhibits a very restricted spatial distribution (< 3 km along and 2 km across the shelf). The depocenter is located off the present-day waterway with a NE-SW orientation, maximum thickness of 3.8 ms and an average value of 1.1 ms (Fig. 10f).

5. Discussion

5.1. Chronostratigraphic framework of deltaic deposits

Both sediment cores penetrate the upper part of U3 (Fig. 11), where the young ages (1774–1776 CE) provide for chronostratigraphic constraints on the formation of the uppermost growth phases of the Adra River deltaic system. According to those ages, it is inferred that U4 and U5 represent more recent features generated during the last two centuries.

The possible time of formation of U1 to U3 are evaluated considering the limited ages at the top of U3, the observed stratigraphic architecture of the deltaic system and the comparison with regional and Mediterranean coastal and deltaic architectures. For example, the interpretation of BSU provides constrains about the older ages of the observed deltaic units. BSU exhibits a patchy distribution, in contrast to the well-defined seaward thinning distributions of overlying units. This pattern would indicate no well-defined relationship with any point sources, and has been interpreted in other shelf settings as the result of estuarine-to-coastal deposition and/or reworking during transgressive conditions (Liu et al., 2009a, 2009b; Choi et al., 2016). Other stratigraphic characteristics of BSU such as widespread distribution, prevalence sheet external shapes and sub-parallel configurations with local onlaps seem also be more compatible by overall sea-level rise conditions. In contrast, overlying units exhibit characteristic progradational patterns, usually related to establishment of deltaic lobes under highstand conditions (e.g., Liu et al., 2017; Chen et al., 2021, 2023). Based on those evidences, we interpret BSU as remnants of coastal deposits formed in a transgressive context; indeed, beach deposits formed during the postglacial sea level rise have also been described in other shelf areas of the northern Alboran margin (Hernández-Molina et al., 1994). Therefore, the change from BSU to the overlying units with dominant prograding geometry is compatible with a transition from transgressive to highstand deposition. Consequently, we estimate that the time of formation of U1 to U3 postdate 7.4 ka, the time of maximum flooding in the coasts of southern Spain (Goy et al., 2003).

The ages obtained at the top of U3 also provide temporal constrains about its formation. Sedimentation rates obtained from sediment core MS-V9 are slightly higher than 1 m/100 years. At that location, U3 is

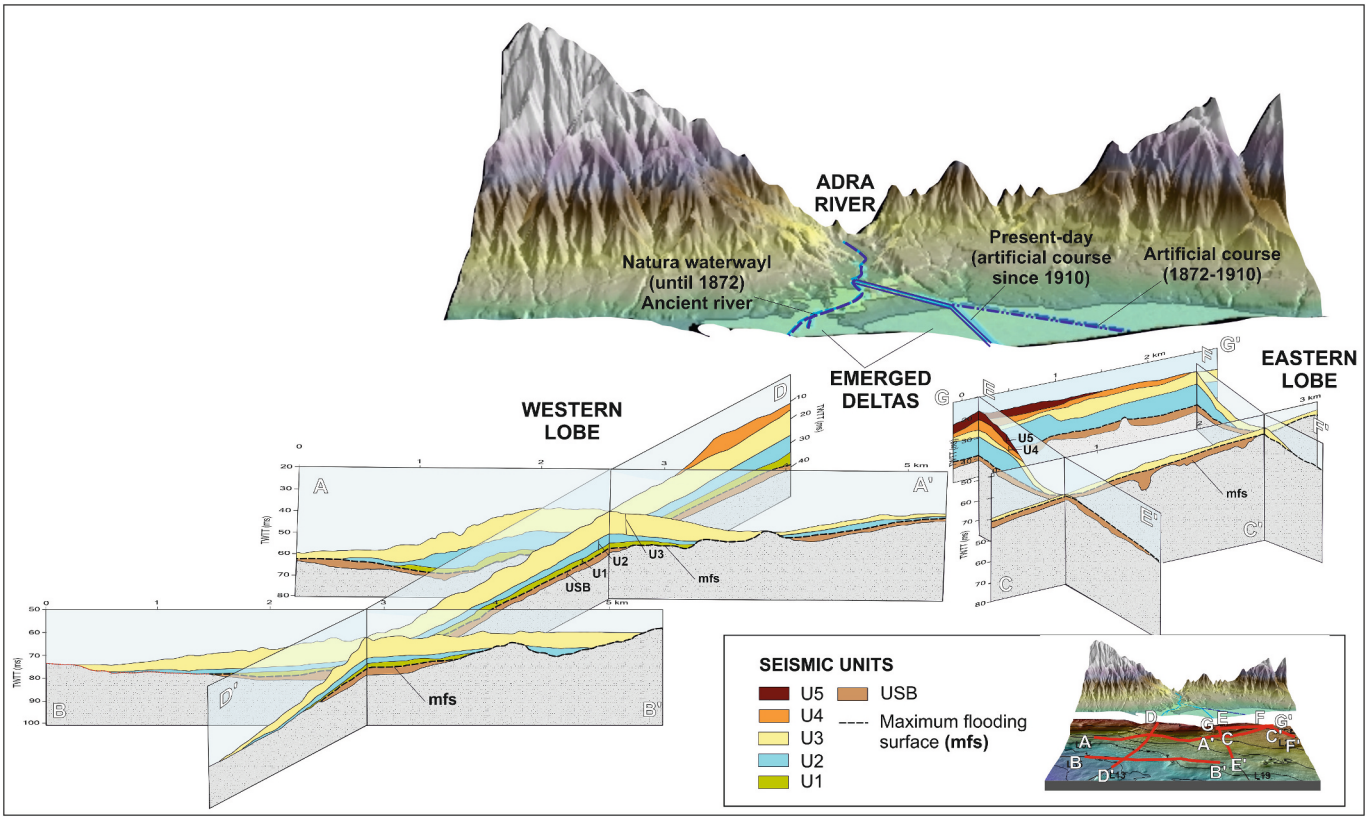

Fig. 8. 3D reconstruction of the architectures of the western and eastern lobes in the subaqueous system of the Adra delta. Most of the growth of the submarine deposits took place during the deposition of units U2 and U3.

around 5 m thick. Extrapolating those sedimentation rates below the bottom part of sediment core MS-V9 towards the lower boundary of U3 at the MS-V9 location, an estimated age of 1390 CE is obtained for the onset of U3. In spite of uncertainties in relation with the assumption of constant sedimentation rates, those estimates are compatible with major development of U3 during the Little Ice Age (LIA). Accordingly, a significant clinoform just a few hundred years old has been correlated in several settings with the LIA (Liu et al., 2013), which was imprinted on deltaic architecture by modifying the role played by dominant processes (Cattaneo et al., 2003; Correggiari et al., 2005a; Sacchi et al., 2009), eventually leading to the most significant deltaic progradation (Di Bella et al., 2014; Fanget et al., 2014).

Although we do not have direct age control for U1 and U2, some tentative chronologies can be proposed considering the age constrains derived from BSU and U3, and the comparison with major regional phases of coastal progradation and major phases of deltaic development in the Mediterranean realm. Regionally, three major coastal progradational phases have been recognized in the Roquetas coastal spit system, located at a short distance (i.e., 10–20 km) east of the Adra deltaic system (Fig. 12). These phases have been related to increased coastal sediment input during high relative sea levels, and are limited by erosional swales formed during periods of increased aridity (Goy et al., 2003). Around the Mediterranean Basin, several major broad phases of deltaic development have been reported. A delta inception phase began with highstand sea level stabilization, and declined at about 4 ka due to intensification of human activities (Anthony et al., 2014). The past 3000 years have witnessed a phase of synchronous delta formation more strongly mediated by human activities. Within this last interval, two major delta inception phases are documented: the first is related to the apex of the Roman Empire, followed by a resumed phase of deltaic progradation during the Renaissance Period that peaked during the LIA (Maselli and Trincardi, 2013; Anthony et al., 2014). Considering the existing regional knowledge concerning sediment production driven by middle to late Holocene cyclicity, we suggest that progradational phases U1 to U3 could be equivalent to the major phases of Mediterranean deltaic growth and the nearby coastal progradational phases.

Those progradational phases could be framed in a regional context characterized by rapid climatic changes at millennial timescales during the middle to Late Holocene, which have been detected in the western Mediterranean through the comparison of multiple marine, lacustrine and fluvial archives (Fletcher and Zielhofer, 2013) (Fig. 12). In particular, the alternance of aridification phases and more humid climatic periods took place in the southeastern Iberian Peninsula throughout the Holocene (Jalut et al., 2000). We postulate that the Adra delta growth phases could have been fostered by mid- and late-Holocene humid periods and the LIA, likewise dominated by recurrent wet conditions (Figs. 11 and 12).

5.2. *Transformation of the submarine deltaic environment: Balance between natural processes and anthropic actions*

5.2.1. *The natural delta with increasing anthropic influence*

The three lower units, U1 to U3, display homogeneous and relatively thick proximal depocenters that thin seaward. Considering the nature of the sedimentary environment under scrutiny, these seismic units can be regarded as the subaqueous portion of individual delta lobe depocenters (Trincardi et al., 2004). Limited sedimentological data in the upper part of unit U3 reveals the dominance of silty sands with intercalated sandy layers. The lithology is similar to other Mediterranean high-energy prodeltaic environment episodically influenced by gravity flows (e.g., Sacchi et al., 2009); specifically, the occurrence of grain-size increases has been related to the influence of extreme floods (Fanget et al., 2014). Besides, the identification of undulatory bedforms at the top of the unit also agrees with deposition by enhanced fluvial flows (Bárcenas et al.,

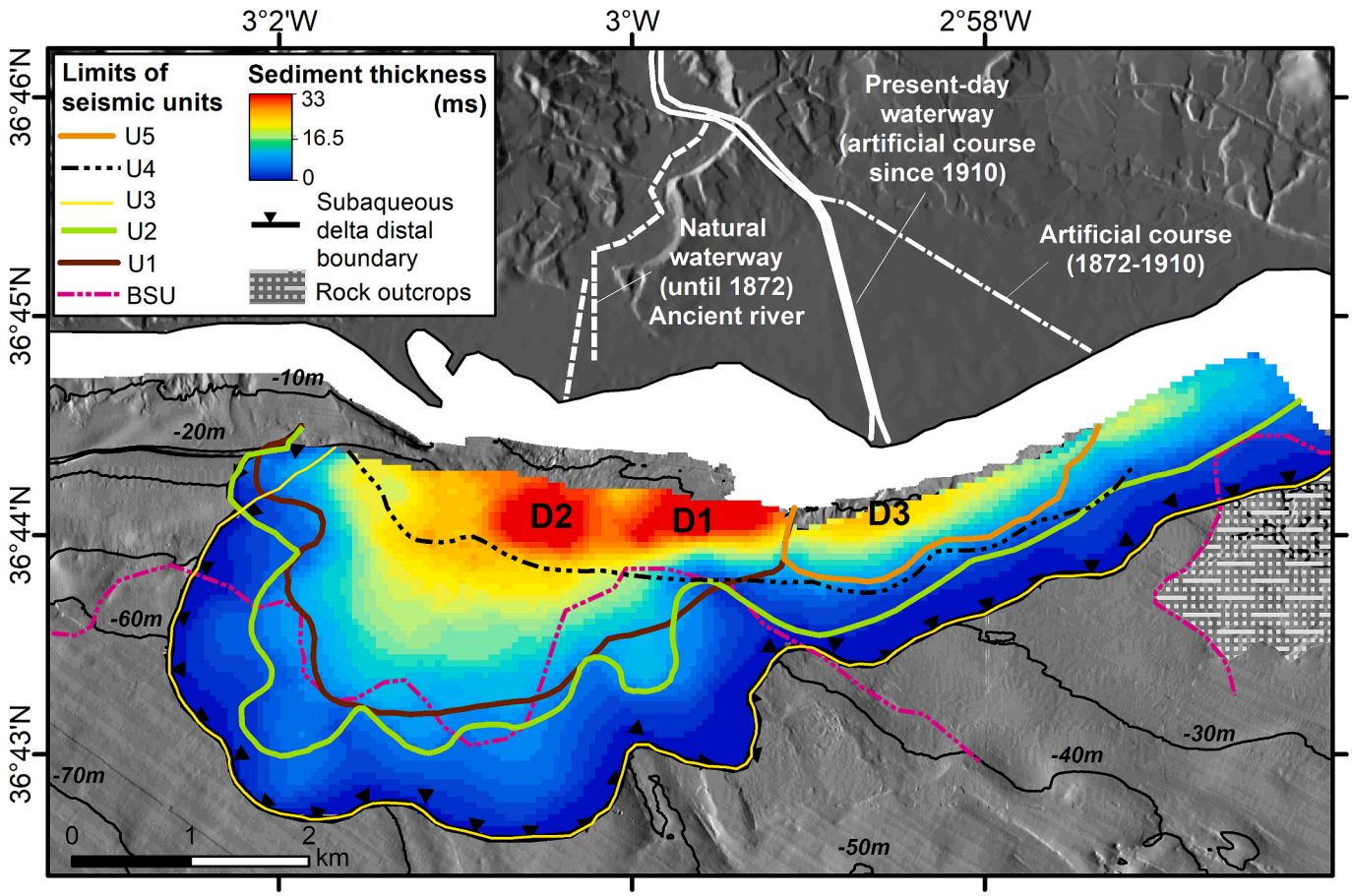

Fig. 9. Bulk sediment thickness map (in milliseconds) of the submarine Adra deltaic system showing the location of the main depocenters (D1 to D3). The seaward boundary of each unit (SBU and U1-U5) is also traced.

2009), as interpreted in other Mediterranean prodeltaic settings (Di Bella et al., 2021; Clementucci et al., 2022). These features are compatible with increased fluvial inputs and the initiation of widespread deltaic progradation during the Holocene highstand (Stanley and Warne, 1994; Liu et al., 2009a, 2009b; Fanget et al., 2014; Choi et al., 2016).

Constructional lobe U1 represents the inception of major deltaic growth in the Adra deltaic system (Fig. 13a). Its distribution pattern is compatible with a phase of more restricted progradation in comparison with subsequent outbuilt phases. The U1 distribution is characteristic of a fluvial-dominated delta formed under high sediment supply conditions (Besset et al., 2017).

Like U1, stratigraphic units U2 and U3 exhibit lobated distributions off the ancient river mouth, in agreement with the long-term development of a triangular delta (Jabaloy-Sánchez et al., 2010). The overall trend of increased subaqueous deltaic development from U1 to U3 may be the result of more efficient humid periods acting over a long-lasting aridification trend. The growing aridity was accompanied by a greater incidence of fires and the reduction in vegetation cover (Carrión et al., 2003), exacerbated by the rise of human occupation (Gil-Romera et al., 2010). Each successive instauration of humid periods would act over more erodible, unprotected substrates and would mobilize higher amounts of sediments.

U2 and U3 also exhibit elongated patterns in the eastern lobe (Fig. 13b and c). The changing lateral distribution patterns from U1 to U2-U3 could reflect a fluvial supply modification to finer-grained sediments, and/or an intensification of longshore sediment transport. We favour the latter hypotheses, as in the eastern distribution area, U2 and U3 sublobes exhibit high-angle tangential oblique configurations, limited offshore progradation, and linear distributions (Figs. 6 and S3). These features are indicative of the formation of coarse-grained depocenters on the downdrift side of the active deltaic outlet. Such distribution patterns indicate an effective littoral drift and wave action (Korus and Fielding, 2015), as small deltas are more influenced by waves during their evolution (Anthony, 2015). Consequently, a transport pattern parallel to the strike of the foresets is established (Cattaneo et al., 2003), which causes a downcurrent deflection and loss of the original deltaic symmetry (Liu et al., 2013; Korus and Fielding, 2015; Ayranci and Dashtgard, 2016). Besides, the observed elongated patterns of U2 and U3 in the eastern depocenter can be related to the entrance of SAW over shallow waters in the study area, causing eastward-directed littoral dynamics under the dominance of westerlies. According to this interpretation, the Adra submarine deltaic system may be regarded as a source area for the Campo de Dalías beach ridge complex, since the eastward-directed sediment transport was active throughout most of the Holocene highstand along the littoral system located to the east of the study area (Goy et al., 2003).

In light of our interpretation, during phases of lobe construction there would have been a coupling between increased rainfalls and wind (i.e., westerlies) dominance. This connection is similar to the pattern established across the Mediterranean region under a negative North Atlantic Oscillation; these phases have been related to increased rainfall and river discharges, due to the eastward displacement of high-intensity storms (e.g., Maas and Macklin, 2002; Struglia et al., 2004; Pociask-Karteczka, 2006).

5.2.2. *Recent evolution and associated morphological changes*

The significant decreases in fluvial inputs and the transition into

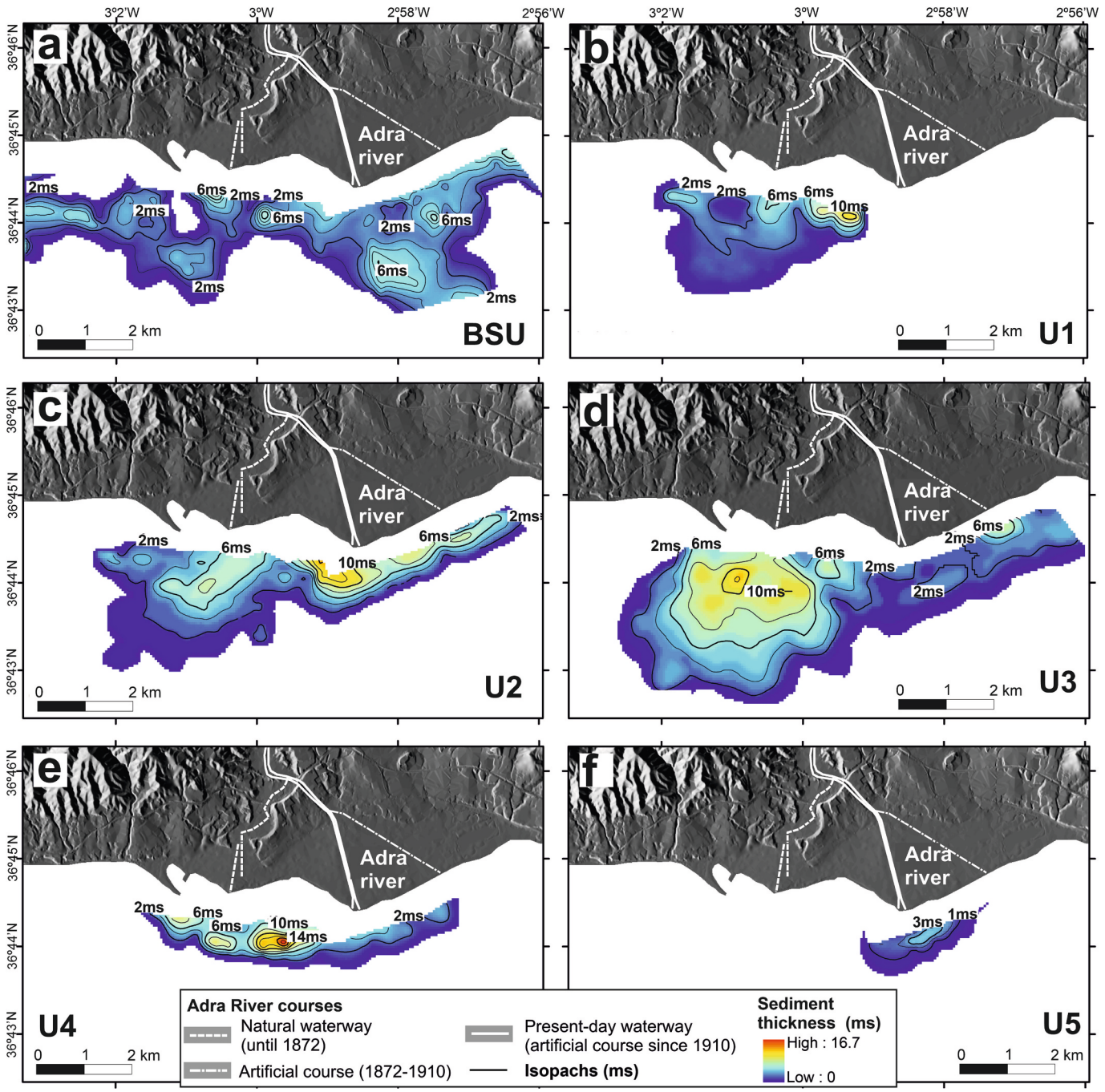

Fig. 10. Sediment thickness maps (in milliseconds) of individual seismic units composing the Adra subaqueous delta. a) BSU; b) U1; c) U2; d) U3; e) U4 and f) U5.

destructional phases of deltaic systems can be seen as global phenomena (e.g., Jiang et al., 2017; Maloney et al., 2018). Since 1800 CE, the sediment supply reduction in the Mediterranean region has been triggered by several anthropogenic activities in the catchments, including agricultural decline, reforestation and engineering works in the channels (Anthony et al., 2014). As a consequence, most Mediterranean deltaic systems are subjected to erosion (Besset et al., 2017). The regulation of drainage basins by dams further results in significant decreases in sediment discharges due to sediment trapping and leads to grain size increase of sediments deposited in the nearshore (Bi et al., 2014; Yang et al., 2018; Ben Moussa et al., 2019).

Such interventions also enhance the erosional effect of waves, favouring the reworking of abandoned deltaic lobes and the asymmetric shaping of deltaic systems, which may become deflected and/or straightened (Correggiari et al., 2005a, 2005b; Anthony, 2015). Elsewhere, deltaic lobes abandoned after anthropic channel diversion have undergone erosion accompanied by shoreline retreat during the last two centuries (Correggiari et al., 2005a, 2005b; Liu et al., 2013; Garcés et al., 2023), with concomitant lateral changes of main depositional areas. Most of these eroded sediments tend to be redeposited in nearby regions, either offshore or in coastal areas, depending on local hydrodynamic conditions (Zhou et al., 2014) and/or the location of newly established river outlets (Jiang et al., 2017).

In the study area, a strong modification of main sedimentation areas during the time of U4-U5 formation is evidenced (Fig. 13d and e). Both U4 and U5 exhibit marked elongated and rather restricted distributions, which suggests a shortage of sediments and increased influenced of wave processes (Ayranci and Dashtgard, 2016); indeed, a drastic change

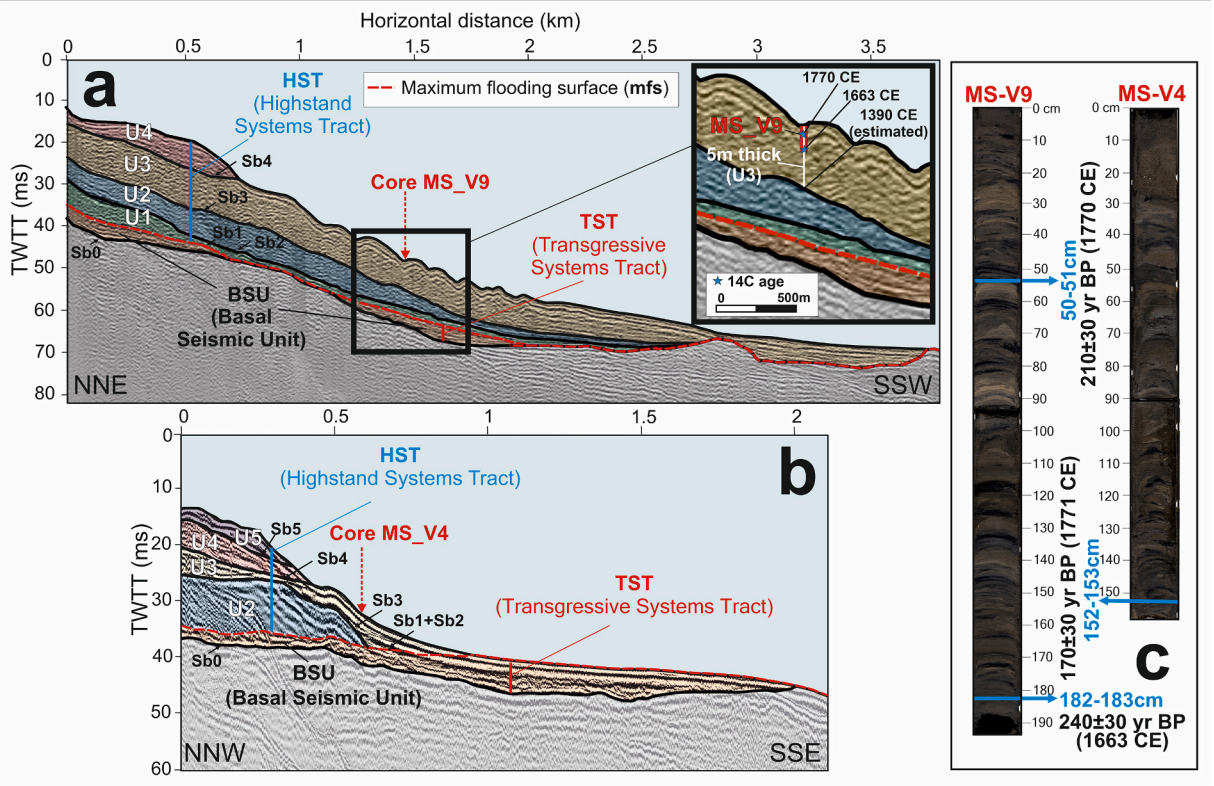

Fig. 11. Architecture and sequence stratigraphy interpretation of the western lobe (a) and the eastern lobe (b) of the Adra subaqueous deltaic system (Adapted from Mendes et al., 2015). Core sites are shown, together with the major seismic units (BSU and U1 to U5) and bounding unconformities (Sb0 to Sb5). A zoom around the location of sediment core MS_V) highlights the total thickness of U3 at that location, the available ages and the estimated age for the base of U3 by extrapolating sedimentation rates. (c) Photographs of sediment cores MS-V9 and MS-V4 acquired in the submarine deltaic system. Location of seismic profiles and sediment cores indicated in Fig. 1b.

to a wave-dominated morphology driven by anthropogenic actions is also observed in the Rhone subaqueous delta (Fanget et al., 2014). The seismic facies and distributions of U4 and U5 resemble infralittoral prograding wedges recognized along the northern Alboran margin; these are deposits developed in areas with minor fluvial supplies and mainly generated by storm-generated downwelling or by longshore currents (e.g., Fernández-Salas et al., 2009; Ortega-Sánchez et al., 2014).

More detailed insights concerning the most recent anthropogenic phase are derived from evidence of recent bathymetric changes (Fig. 2). Decreased bathymetries in the western prodeltaic lobe off the ancient river mouth are interpreted as the result of erosion since the first river channel deviation. An alternative would be to consider those bathymetric changes as the result of migrating bedform fields; however, this hypothesis seems to be incompatible with a dearth of fluvial fluxes. In contrast, most of the eastern area has been accreting, particularly the most proximal area where U4 and U5 occur. The more recent decadal changes furthermore suggest that the older deltaic lobe is mainly eroding, particularly along the steep foresets. Yet there are some depositional areas over the topsets of the older deltaic bulge; in addition, the area covered by U4-U5 is actively accreting.

All this evidence suggests a significant change in the depositional dynamics and a pronounced imprint of anthropic activity on the deltaic system during the last two centuries. The most recent deltaic regime exhibits a strong hydrodynamic control and very reduced fluvial supply. A significant dearth of sediment supply to the older (western) subaqueous deltaic lobe took place, and part of the eroded sediment could have been entrained by longshore dynamics feeding sediments to the more recent wedges. Indeed, the subsequent sediment transport by waves and longshore currents favoured the formation of a main elongated proximal depocenter and a secondary off-shelf deposit.

5.3. *Spatial variability of composite architectures of Holocene submarine deltas: Genetic implications*

Composite architectures of recent subaqueous deltaic clinothems have been observed in several major deltaic environments, such as the Ganges-Brahmaputra (Palamenghi et al., 2011), the Yellow (Liu et al., 2009a, 2009b, 2013), and the Yangtze river deltas (Feng et al., 2016; Xu et al., 2016), as well as the Gulf of Papua (Slingerland et al., 2008). In the Mediterranean Sea, several major deltaic depocenters —the Po River delta (Correggiari et al., 2005a) and its lateral extension off the Gargano promontory (Cattaneo et al., 2003), or the Rhone subaqueous delta (Fanget et al., 2014)— and some smaller deltaic systems and fan deltas (Sacchi et al., 2009; Di Bella et al., 2014) also exhibit a multi-phased stratigraphy.

Deltaic depositional units formed during the Holocene stillstand generally reflect the imprint of river basin changes driven by natural processes. In particular, the alternance of humid and dry phases influences the frequency of flood events and ultimately may impact sediment supply (Sacchi et al., 2009; Xu et al., 2016) and sedimentation rates (Palamenghi et al., 2011). In other cases, however, changes in sea level rise and/or sediment supply rates induced by subsidence may explain the observed geometries (Slingerland et al., 2008; Fanget et al., 2014; Feng et al., 2016). In contrast, the influence of human actions on submarine deltaic composite architectures has been rarely documented.

The constructional blocks of the Adra submarine delta point to Late Holocene trends that leave an imprint both in the stratigraphic architecture and the distribution patterns. Since a relationship may be established between flood events and deltaic progradational phases during the last few millennia (Sacchi et al., 2009; Milli et al., 2013), the seismic stacking pattern of the Adra subaqueous deltaic system is

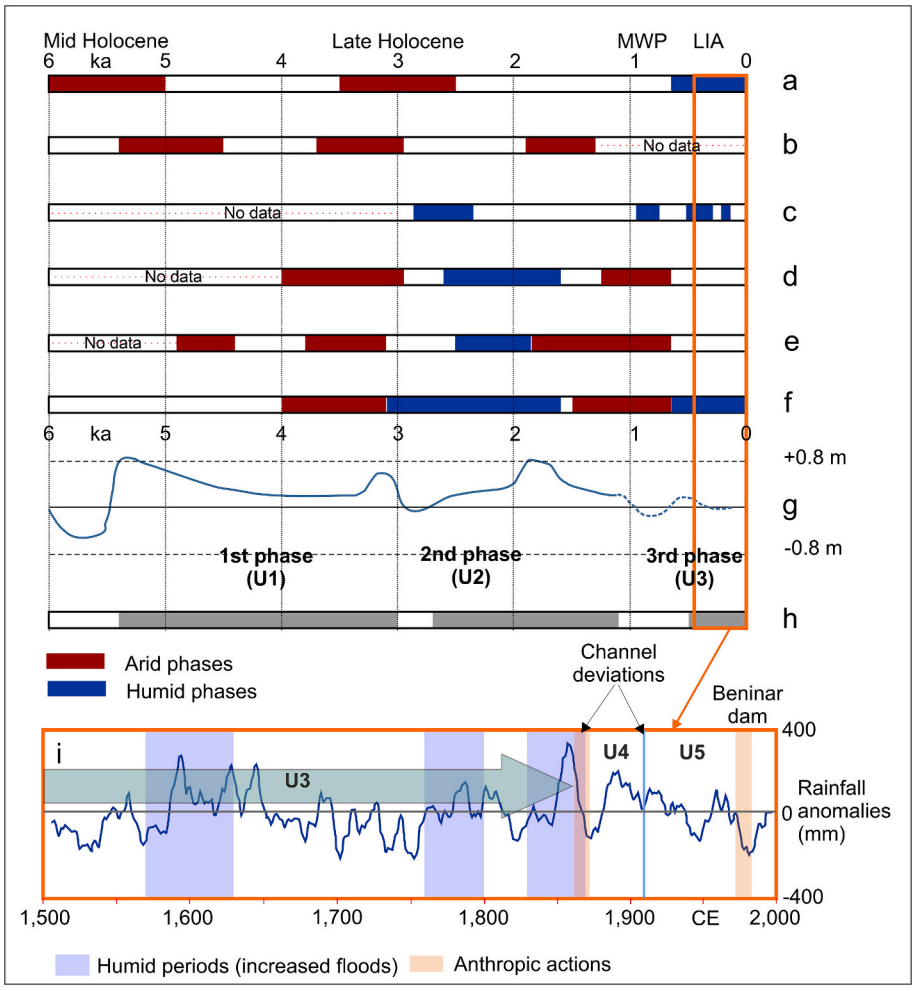

Fig. 12. Correlation panel of different climatic and sedimentary events recorded in the Mediterranean Basin and the southeastern Iberian Peninsula. The different phases of deltaic build up recognized in the subaqueous Adra delta (U1 to U5) are tentatively correlated with known climatic events during the last 6 ka. Humid phases are associated with intervals of increased frequency/intensity of flood events. of the ages of these events are derived from the following sources: a) Fletcher and Zielhofer (2013); b) Fletcher et al. (2013); c) Benito et al. (2008); d) Martín-Puertas et al. (2008); e) Jiménez-Moreno et al. (2013) and Navarro-Hervás et al. (2014); f) Ramos-Román et al. (2016) g) Relative sea-level changes deduced from beach ridge progradational patterns in the Campo de Dalías, located 10–30 km east of the Adra River delta (Goy et al., 2003). h) Major coastal progradations in the Campo de Dalías (Goy et al., 2003). i) Rainfall anomalies in southern Spain during the last 500 yr; periods of increased floods and main interventions in the Adra River are marked (Rodrigo et al., 2000). MWP: Medieval Warm Period; LIA: Little Ice Age.

compatible with episodic deltaic growth and cyclic progradation. The formation of individual prodelta lobes (i.e., the identified seismic units) would have been favoured by phases of increased supply during humid periods (Fig. 13). The potential influence of recent sea level and/or subsidence changes appears to be of minor relevance in the study area, given the steep physiography and dominant uplifting trend (Galve et al., 2020) of the margin and the overall low dimensions of the entire system.

Internal bounding surfaces within the highstand phases of subaqueous deltas are regarded as the product of intervals of reduced deposition or bypass (Cattaneo et al., 2003; Slingerland et al., 2008), or even erosional periods triggered either by shifting river mouths that cause the abandonment of deltaic lobes (Fielding et al., 2006; Liu et al., 2013), by abandoned lobes which can substantially modify oceanographic conditions or extend coastal dynamics (Correggiari et al., 2005b; Lavoie et al., 2014), or by man-made structures such as dams or channel fixations, which tend to promote erosional processes in subaqueous deltas (Correggiari et al., 2005b; Yang et al., 2011). In the study area, we propose that the boundaries of prodeltaic lobes could represent non-depositional surfaces reflecting drastic changes of sediment supplies.

A detailed reconstruction of subaqueous deltaic lobes featuring distribution thickness maps for each lobe is rarely achieved (e.g., Fanget et al., 2014, for the Rhone subaqueous delta). The temporal evolution of the successive lobes provides significant insights regarding the governing processes (Fig. 13). In wider, more extensive deltaic systems, lateral depocenter redistribution is usually the product of successive river avulsion and delta lobe switching processes (Correggiari et al., 2005a, 2005b; Fielding et al., 2006; Flocks et al., 2006; Liu et al., 2009a, 2009b; Fanget et al., 2014). However, clear evidence of similar processes in the study area are lacking; the lobate depocenters of the Adra deltaic system persisted in a similar location off the ancient river mouth during their development. It is suspected that the physiographic control dictated by the Betic Mountains prevented river avulsion, due to the steep, rocky nature of the Adra catchment. Instead, the individual subaqueous delta lobes of the Adra deltaic system would have undergone significant lateral changes in depocenter distribution. Thus, they evolved from markedly lobate, indicative of strong fluvial influence, to markedly elongate, indicative of strong lateral redistribution by longshore drift and wave dominance. Similar changes from fluvial to wave dominance have been documented in other subaqueous deltaic environments, in response to sediment supply changes driven by climatic changes and by anthropic factors (Fanget et al., 2014).

This trend is apparent in the distribution maps from U1 to U5 (Figs. 10 and 13) and can also be related to the interplay between

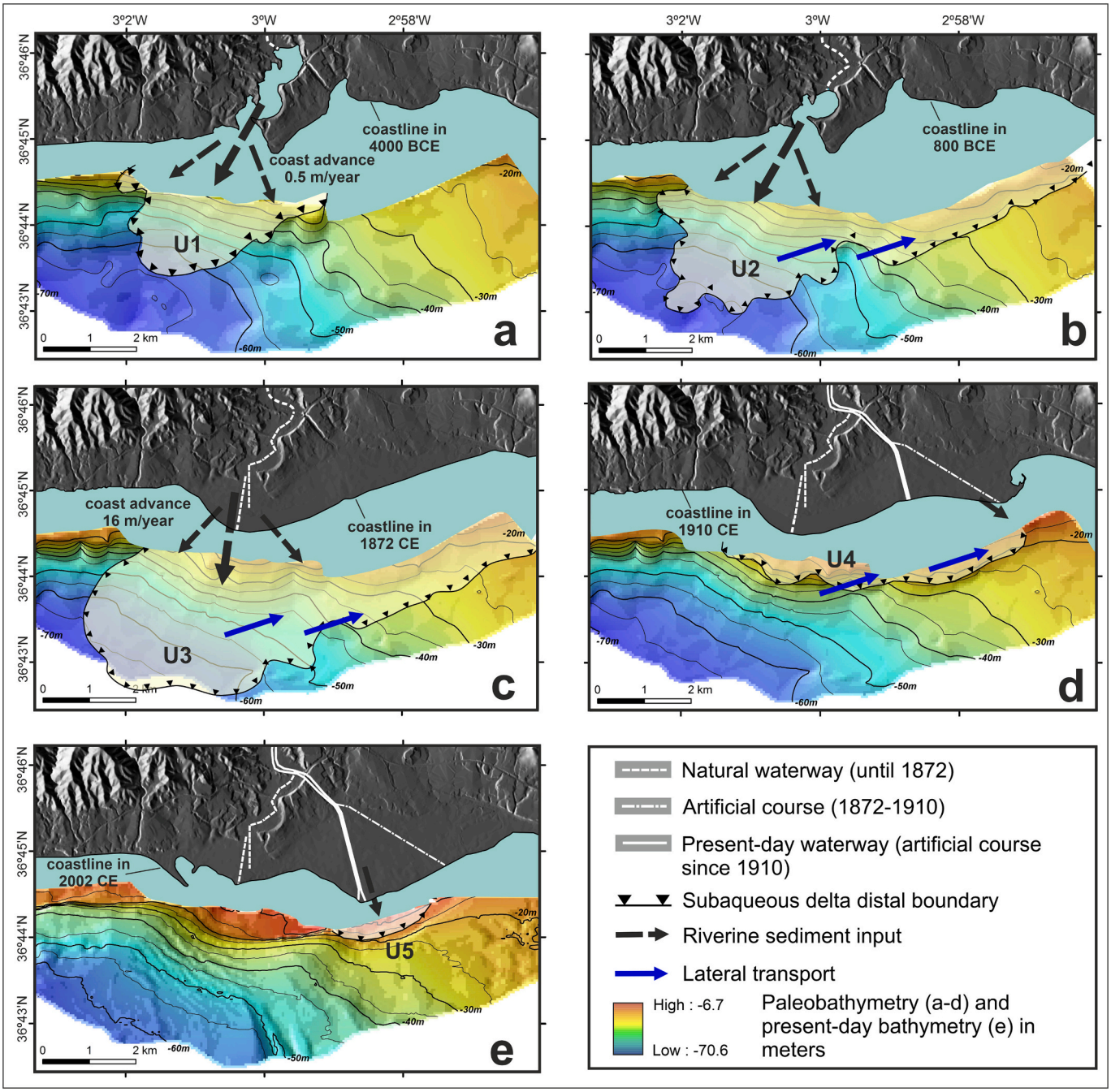

Fig. 13. Reconstruction of the successive evolutionary steps of the Adra River subaqueous deltaic system during the Late Holocene highstand. a) Initial formation of a fluvially-dominated prodeltaic lobe at the beginning of the Late Holocene. b) Progradational phase of a deltaic system during the Late Holocene, linked to humid climatic conditions. c) Progradational phase of a deltaic system during the LIA, linked to humid climatic conditions. d) Wave-dominated system after the river channel was artificially deviated in 1872. e) Wave-dominated system after the river channel acquired its present location in 1910.

climatic and anthropic factors: a general aridification trend in south-eastern Iberia since the Middle Holocene (Carrión et al., 2003), punctuated by humid periods, and the growing importance of human activities in the catchment of the Adra River.

6. Conclusions

Reconstruction of the different evolutionary phases of the submarine portion of the Adra River deltaic system documents a Late Holocene morphological change —from a former fluvially-dominated lobate delta to presentwave-dominated elongated deltaic deposits. The progressive transformation of the entire deltaic system is attributed to a prolonged aridification trend during the Holocene highstand, punctuated by humid phases when progradational events were favoured. Over time, anthropogenic modifications in the river drainage basin caused a dearth of sediment flux to the deltaic system. The prevalence of climatic versus anthropogenic influence in the deltaic system marks two major evolutionary phases: the first mediated by the instauration of a dominant climatic cyclicity during the middle to Late Holocene, and a recent one strongly conditioned by human interventions.

The natural evolution of the system entailed asymmetrical growth of the subaqueous delta during periods of increased sediment supply to the shelf, with the subsequent enhancement of progradational phases. These phases roughly correlate with the major deltaic developments in the

Mediterranean realm and to regional phases of coastal progradation. An eastward-directed longshore transport is ascribed to the entrance of Atlantic water and possibly favoured the growth of lateral beach ridge systems. Therefore, the Adra deltaic system could be regarded as a source area for the coastal sectors in the easternmost northern Alboran Sea margin. The most important progradational phase is apparently connected with the dominance of river flood events during the LIA, and was exacerbated by deforestation in the adjacent hinterlands.

Channel deviation in historical time to prevent river flood events determined a major modification of the distribution of subaqueous deltaic deposits, essentially confined in shallow-water. These deposits grew laterally due to partial ravinement of the older deltaic system, the action of waves and longshore sediment redistribution. The last phase, involving the latest river mouth, was influenced by river damming and deltaic growth. Small deltaic systems such as that of the Adra River are thus shown to be particularly sensitive systems that record interactions between natural processes, such as fluviatile inputs and longshore sediment dynamics, and anthropogenic modification, which in general terms tend to diminish sediment flux to the system.

Supplementary data to this article can be found online at https://doi.org/10.1016/j.margeo.2024.107386.

CRediT authorship contribution statement

P. Bárcenas: Writing – review & editing, Writing – original draft, Investigation, Formal analysis. **F.J. Lobo:** Writing – review & editing, Writing – original draft, Supervision, Conceptualization. **L.M. Fernández-Salas:** Writing – review & editing, Supervision, Funding acquisition. **I. Mendes:** Writing – review & editing, Formal analysis. **N. López-González:** Writing – review & editing. **J. Macías:** Writing – review & editing, Funding acquisition.

Declaration of competing interest

The authors declare that they have no known competing financial interests or personal relationships that could have appeared to influence the work reported in this paper.

Data availability

The data used in this study are posted in DIGITAL.CSIC repository (https://digital.csic.es/) with the following DOI: https://doi.org/10.20350/digitalCSIC/15706. The owner of these data is the Spanish Institute of Oceanography - CSIC and any other type of data not incorporated in the repository can be accessed on demand.

Acknowledgments

This work was completed thanks to the following projects supported by the Junta de Andalucía: “Modelado, simulación numérica y análisis del transporte de sedimentos en los abanicos submarinos de los ríos de Andalucía oriental”—MOSAICO (P06-RNM-01594), “Transporte de Sedimentos en la Plataforma Continental de Andalucía Oriental: Observación Multiescalar, Modelado y Simulación Numérica”—TESELA (P11-799 RNM7069) and “Evolución reciente de los contactos principales entre dominios estructurales/reológicos del Sistema del Arco de Gibraltar: estudios integrados tierra-mar” (RNM-451). It was also supported by the project entitled Alboran Shelf-Slope cOupling processes and deep sediMent trAnsfeR: Source To Sink approaches and implications for biodiversity— ALSSOMAR S2S (CTM2017-88237-P), funded by the Ministerio de Economía y Competitividad, Spain. I. Mendes thanks to Fundação para a Ciência e a Tecnologia for contracts DL57/2016/CP1361/CT0009, CEECINST/00052/2021/CP2792/CT0012, projects UID/0350/2020 CIMA and LA/P/0069/2020. Database used in this study is stored in the IEO institutional repository, and can be accessed on demand. The English style of the manuscript was reviewed by Jean Sanders. Three external reviewers provided extensive comments and suggestions that improved considerably the initial version of the manuscript.

References

Albérola, C., Rousseau, S., Millot, C., Astraldi, M., Font, J., Garcia-Lafuente, J., Gasparini, G.P., Send, U., Vangriesheim, A., 1995. Tidal currents in the western Mediterranean Sea. Oceanol. Acta 18 (2), 273–284.

Anthony, E.J., 2014a. Deltas. In: Masselink, G., Gehrels, R. (Eds.), Coastal Environments and Global Change. American Geophysical Union, Somerset, GB, pp. 299–337.

Anthony, E.J., 2014b. The Human influence on the Mediterranean coast over the last 200 years: a brief appraisal from a geomorphological perspective. Géomorphologie 20 (3), 219–226. https://doi.org/10.4000/geomorphologie.10654.

Anthony, E.J., 2015. Wave influence in the construction, shaping and destruction of river deltas: A review. Mar. Geol. 361, 53–78. https://doi.org/10.1016/j.margeo.2014.12.004.

Anthony, E.J., Marriner, N., Morhange, C., 2014. Human influence and the changing geomorphology of Mediterranean deltas and coasts over the last 6000 years: from progradation to destruction phase? Earth Sci. Rev. 139, 336–361. https://doi.org/10.1016/j.earscirev.2014.10.003.

Ayranci, K., Dashtgard, S.E., 2016. Asymmetrical deltas below wave base: insights from the Fraser River Delta, Canada. Sedimentology 63 (3), 761–779. https://doi.org/10.1111/sed.12237.

Bárcenas, P., Fernández-Salas, L.M., Macías, J., Lobo, F.J., Díaz del Río, V., 2009. Estudio morfométrico comparativo entre las ondulaciones de los prodeltas de los ríos de Andalucía Oriental. Rev. Soc. Geol. Esp. 22 (1–2), 43–56.

Bárcenas, P., Lobo, F.J., Macías, J., Fernández-Salas, L.M., Díaz del Río, V., 2011. Spatial variability of surficial sediments on the northern shelf of the Alboran Sea: the effects of hydrodynamic forcing and supply of sediment by rivers. J. Iber. Geol. 37 (2), 195–214. https://doi.org/10.5209/rev_JIGE.2011.v37.n2.8.

Barriendos Vallve, M., Martin-Vide, J., 1998. Secular climatic oscillations as indicated by catastrophic floods in the Spanish Mediterranean Coastal Area (14th–19th Centuries). Clim. Chang. 38 (4), 473–491. https://doi.org/10.1023/A:1005343828552.

Benito, G., Thorndycraft, V.R., Rico, M., Sánchez-Moya, Y., Sopeña, A., 2008. Palaeoflood and floodplain records from Spain: evidence for long-term climate variability and environmental changes. Geomorphology 101 (1–2), 68–77. https://doi.org/10.1016/j.geomorph.2008.05.020.

Besset, M., Anthony, E.J., Sabatier, F., 2017. River delta shoreline reworking and erosion in the Mediterranean and Black Seas: the potential roles of fluvial sediment starvation and other factors. Elementa 5 (54). https://doi.org/10.1525/journal.elementa.139.

Besset, M., Anthony, E.J., Bouchette, F., 2019. Multi-decadal variations in delta shorelines and their relationship to river sediment supply: an assessment and review. Earth Sci. Rev. 193, 199–219. https://doi.org/10.1016/j.earscirev.2019.04.018.

Bi, N., Wang, H., & Yang, Z. (2014). Recent changes in the erosion–accretion patterns of the active Huanghe (Yellow River) delta lobe caused by human activities. Cont. Shelf Res., 90(0), 70–78. doi:https://doi.org/10.1016/j.csr.2014.02.014.

Carrión, J.S., Sánchez-Gómez, P., Mota, J.F., Yll, R., Chaín, C., 2003. Holocene vegetation dynamics, fire and grazing in the Sierra de Gádor, southern Spain. The Holocene 13 (6), 839–849. https://doi.org/10.1191/0959683603hl662rp.

Carvajal, R., Sanz de Galdeano, C., 2008. Aplicación de índices geomorfológicos al estudio de la cuenca del río Adra (Almería). Cuaternario y Geomorfol 22 (1–2), 17–31.

Casalbore, D., Biancone, M., Casas, D., Mata, P., Alonso, B., Ercilla, G., Chiocci, F.L., Bárcenas, P., López-González, N., 2022. Holocene morpho-stratigraphic evolution of a compound submarine deltaic system in front of the shelf-incising Almanzora and Garrucha Canyons (Palomares margin, southeastern Iberia). Mar. Geol. 444, 106708 https://doi.org/10.1016/J.MARGEO.2021.106708.

Cattaneo, A., Correggiari, A., Langone, L., Trincardi, F., 2003. The late-Holocene Gargano subaqueous delta, Adriatic shelf: sediment pathways and supply fluctuations. Mar. Geol. 193 (1–2), 61–91. https://doi.org/10.1016/S0025-3227(02)00614-X.

Cattaneo, A., Trincardi, F., Langone, L., Asioli, A., Puig, P., 2004. Clinoform generation on Mediterranean Margins. Oceanography 17, 105–117. https://doi.org/10.5670/oceanog.2004.08.

Cattaneo, A., Trincardi, F., Asioli, A., Correggiari, A., 2007. The Western Adriatic shelf clinoform: energy-limited bottomset. Cont. Shelf Res. 27 (3–4), 506–525. https://doi.org/10.1016/j.csr.2006.11.013.

Chen, Y., Deng, B., Chen, Y., Wang, D., Zhang, J., 2021. Holocene sedimentary evolution of a subaqueous delta off a typical tropical river, Hainan Island, South China. Mar. Geol. 442, 106664 https://doi.org/10.1016/J.MARGEO.2021.106664.

Chen, Y., Deng, B., Saito, Y., Wang, Z., Yang, X., Wu, J., 2023. Pearl River sediment dispersal over its associated delta–estuary–shelf system during the Holocene. Sedimentology 70 (7), 2331–2354. https://doi.org/10.1111/SED.13123.

Choi, D.-L., Lee, Y.-K., Shin, D.-H., Woo, H.-J., 2016. Holocene depositional patterns of the subaqueous Nakdong Delta on the Korea Strait with respect to sequence stratigraphy. Ocean Sci. J. 51 (2), 251–261. https://doi.org/10.1007/s12601-016-0021-0.

Clementucci, R., Lafosse, M., Casalbore, D., Ridente, D., d’Acremont, E., Rabaute, A., Chiocci, F.L., Gorini, C., 2022. Common origin of coexisting sediment undulations and gullies? Insights from two modern Mediterranean prodeltas (southern Italy and

northern Morocco). Geomorphology 402, 108133. https://doi.org/10.1016/J.GEOMORPH.2022.108133.
Correggiari, A., Cattaneo, A., Trincardi, F., 2005a. The modern Po Delta system: Lobe switching and asymmetric prodelta growth. Mar. Geol. 222-223, 49–74. https://doi.org/10.1016/j.margeo.2005.06.039.
Correggiari, A., Cattaneo, A., Trincardi, F., 2005b. Depositional patterns in the Late Holocene Po Delta System. In: Giosan, L., Bhattacharya, J.P. (Eds.), River Deltas-Concepts, Models, and Examples, SEPM Special Publication, vol. 83. SEPM (Society for Sedimentary Geology), pp. 365–392.
Cuéllar Villar, D., 2006. Historia de una obra pública: la desviación del río Adra (1862-1873). Farua, Extra I, 101–112.
Di Bella, L., Frezza, V., Bergamin, L., Carboni, M.G., Falese, F., Martorelli, E., et al., 2014. Foraminiferal record and high-resolution seismic stratigraphy of the Late Holocene succession of the submerged Ombrone River delta (Northern Tyrrhenian Sea, Italy). Quat. Int. 328–329, 287–300. https://doi.org/10.1016/j.quaint.2013.09.043.
di Bella, L., Pierdomenico, M., Bove, C., Casalbore, D., Ridente, D., 2021. Benthic foraminiferal response to sedimentary processes in a prodeltaic environment: the Gulf of Patti case study (Southeastern Tyrrhenian Sea). Geosciences 11 (5). https://doi.org/10.3390/geosciences11050220.
Díaz, J.I., Ercilla, G., 1993. Holocene depositional history of the Fluviá—Muga prodelta, northwestern Mediterranean Sea. Mar. Geol. 111 (1–2), 83–92. https://doi.org/10.1016/0025-3227(93)90189-3.
Duque, C., Calvache, M.L., Pedrera, A., Martín-Rosales, W., López-Chicano, M., 2008. Combined time domain electromagnetic soundings and gravimetry to determine marine intrusion in a detrital coastal aquifer (Southern Spain). J. Hydrol. 349 (3–4), 536–547. https://doi.org/10.1016/j.jhydrol.2007.11.031.
el Bastawesy, M., Gebremichael, E., Sultan, M., Attwa, M., Sahour, H., 2020. Tracing Holocene channels and landforms of the Nile Delta through integration of early elevation, geophysical, and sediment core data. The Holocene 30 (8), 1129–1141. https://doi.org/10.1177/0959683620913928.
Ercilla, G., Alonso, B., 1996. Quaternary siliciclastic sequence stratigraphy of western Mediterranean passive and tectonically active margins: The role of global versus local controlling factors. In: de Batist, M., Jacobs, P. (Eds.), Geology of Siliciclastic Shelf Seas, Geological Society, London, Special Publication, pp. 125–137. https://doi.org/10.1144/GSL.SP.1996.117.01.07. Issue 117.
Fanget, A.S., Bassetti, M.A., Arnaud, M., Chiffoleau, J.F., Cossa, D., Goineau, A., Fontanier, C., Buscail, R., Jouet, G., Maillet, G.M., Negri, A., Dennielou, B., Berné, S., 2013. Historical evolution and extreme climate events during the last 400 years on the Rhone prodelta (NW Mediterranean). Mar. Geol. 346 (0), 375–391. https://doi.org/10.1016/j.margeo.2012.02.007.
Fanget, A.-S., Berné, S., Jouet, G., Bassetti, M.-A., Dennielou, B., Maillet, G.M., Tondut, M., 2014. Impact of relative sea level and rapid climate changes on the architecture and lithofacies of the Holocene Rhone subaqueous delta (Western Mediterranean Sea). Sediment. Geol. 305, 35–53. https://doi.org/10.1016/j.sedgeo.2014.02.004.
Feng, Z., Liu, B., Zhao, Y., Li, X., Jiang, L., Si, S., 2016. Spatial and temporal variations and controlling factors of sediment accumulation in the Yangtze River estuary and its adjacent sea area in the Holocene, especially in the Early Holocene. Cont. Shelf Res. 125, 1–17. https://doi.org/10.1016/j.csr.2016.06.007.
Fernández-Salas, L.M., Lobo, F.J., Hernández-Molina, F.J., Somoza, L., Rodero, J., Díaz del Río, V., Maldonado, A., 2003. High-resolution architecture of Late Holocene highstand prodeltaic deposits from southern Spain: the imprint of high-frequency climatic and relative sea-level changes. Cont. Shelf Res. 23 (11−13), 1037–1054. https://doi.org/10.1016/S0278-4343(03)00120-1.
Fernández-Salas, L.M., Dabrio, C.J., Goy, J.L., Díaz del Río, V., Zazo, C., Lobo, F.J., et al., 2009. Land-sea correlation between Late Holocene coastal and infralittoral deposits in the SE Iberian Peninsula (Western Mediterranean). Geomorphology 104 (1–2), 4–11. https://doi.org/10.1016/j.geomorph.2008.05.013.
Fielding, C.R., Trueman, J.D., Alexander, J., 2006. Holocene depositional history of the Burdekin River Delta of Northeastern Australia: a model for a low-accommodation, Highstand Delta. J. Sediment. Res. 76 (3), 411–428. https://doi.org/10.2110/jsr.2006.032.
Fletcher, W.J., Zielhofer, C., 2013. Fragility of Western Mediterranean landscapes during holocene rapid climate changes. Catena 103, 16–29. https://doi.org/10.1016/j.catena.2011.05.001.
Fletcher, W.J., Debret, M., Goñi, M.F.S., 2013. Mid-Holocene emergence of a low-frequency millennial oscillation in western Mediterranean climate: implications for past dynamics of the North Atlantic atmospheric westerlies. The Holocene 23 (2), 153–166. https://doi.org/10.1177/0959683612460783.
Flocks, J.G., Ferina, N.F., Dreher, C., Kindinger, J.L., Fitzgerald, D.M., Kulp, M.A., 2006. High-resolution stratigraphy of a Mississippi subdelta-lobe progradation in the Barataria Bight, North-Central Gulf of Mexico. J. Sediment. Res. 76 (3), 429–443. https://doi.org/10.2110/jsr.2006.030.
Galindo-Zaldívar, J., Braga, J.C., Marín-Lechado, C., Ercilla, G., Martín, J.M., Pedrera, A., Casas, D., Aguirre, J., Ruiz-Constán, A., Estrada, F., Puga-Bernabéu, Á., Sanz de Galdeano, C., Juan, C., García-Alix, A., Vázquez, J.T., Alonso, B., 2019. Extension in the Western Mediterranean. In: Quesada, C., Oliveira, J.T. (Eds.), The Geology of Iberia: A Geodynamic Approach: Volume 4: Cenozoic Basins. Springer International Publishing, pp. 61–103. https://doi.org/10.1007/978-3-030-11190-8_3.
Galve, J.P., Pérez-Peña, J.V., Azañón, J.M., Insua Pereira, D.M., Cunha, P.P., Pereira, P., Ortuño, M., Viaplana-Muzas, M., Gracia Prieto, F.J., Remondo, J., Jabaloy, A., Bardají, T., Silva, P.G., Lario, J., Zazo, C., Luis Goy, J., Dabrio, C.J., Cabero, A., 2020. Active Landscapes of Iberia. In: Quesada, C., Oliveira, J.T. (Eds.), The Geology of Iberia: A Geodynamic Approach: Volume 5: Volume 5: Active Processes: Seismicity, Active Faulting and Relief. Springer International Publishing, pp. 77–124. https://doi.org/10.1007/978-3-030-10931-8_5.
Garcés, R., Roca, M., Martínez-Clavel, B., Blázquez, A.M., 2023. Long-term bathymetric changes in the submerged delta of the Turia river since the nineteenth century (Western Mediterranean) and their drivers. Sci. Total Environ. 905, 167296 https://doi.org/10.1016/J.SCITOTENV.2023.167296.
García Lafuente, J.M., Lucaya, N.C., 1994. Tidal dynamics and associated features of the northwestern shelf of the Alboran Sea. Cont. Shelf Res. 14 (1), 1–21. https://doi.org/10.1016/0278-4343(94)90002-7.
Gil-Romera, G., Carrión, J.S., Pausas, J.G., Sevilla-Callejo, M., Lamb, H.F., Fernández, S., Burjachs, F., 2010. Holocene fire activity and vegetation response in South-Eastern Iberia. Quat. Sci. Rev. 29 (9–10), 1082–1092. https://doi.org/10.1016/j.quascirev.2010.01.006.
Goy, J.L., Zazo, C., Dabrio, C.J., 2003. A beach-ridge progradation complex reflecting periodical sea-level and climate variability during the Holocene (Gulf of Almería, Western Mediterranean). Geomorphology 50 (1–3), 251–268. https://doi.org/10.1016/S0169-555X(02)00217-9.
Hernández-Molina, F.J., Somoza, L., Rey, J., Pomar, L., 1994. Late Pleistocene-Holocene sediments on the Spanish continental shelves: model for very high resolution sequence stratigraphy. Mar. Geol. 120 (3–4), 129–174. https://doi.org/10.1016/0025-3227(94)90057-4.
Jabaloy-Sánchez, A., Lobo, F.J., Azor, A., Bárcenas, P., Fernández-Salas, L.M., del Río, V. D., Pérez-Peña, J.V., 2010. Human-driven coastline changes in the Adra River deltaic system, Southeast Spain. Geomorphology 119 (1–2), 9–22. https://doi.org/10.1016/j.geomorph.2010.02.004.
Jalut, G., Esteban Amat, A., Bonnet, L., Gauquelin, T., Fontugne, M., 2000. Holocene climatic changes in the Western Mediterranean, from south-East France to south-East Spain. Palaeogeogr. Palaeoclimatol. Palaeoecol. 160 (3), 255–290. https://doi.org/10.1016/S0031-0182(00)00075-4.
Jiang, C., Pan, S., Chen, S., 2017. Recent morphological changes of the Yellow River (Huanghe) submerged delta: causes and environmental implications. Geomorphology 293, 93–107. https://doi.org/10.1016/j.geomorph.2017.04.036.
Jiménez-Moreno, G., García-Alix, A., Hernández-Corbalán, M.D., Anderson, R.S., Delgado-Huertas, A., 2013. Vegetation, fire, climate and human disturbance history in the southwestern Mediterranean area during the Late Holocene. Quat. Res. 79 (2), 110–122. https://doi.org/10.1016/j.yqres.2012.11.008.
Korus, J.T., Fielding, C.R., 2015. Asymmetry in Holocene river deltas: patterns, controls, and stratigraphic effects. Earth Sci. Rev. 150, 219–242. https://doi.org/10.1016/j.earscirev.2015.07.013.
Lario, J., Zazo, C., Goy, J.L., 1999. Fases de progradación y evolución morfosedimentaria de la flecha litoral de Calahonda (Granada) durante el Holoceno. Estud. Geol. 55, 247–250.
Lavoie, C., Jiménez, J.A., Canals, M., Lastras, G., De Mol, B., Amblas, D., et al., 2014. Influence on present-day coastal dynamics and evolution of a relict subaqueous delta lobe: Sol de Riu lobe, Ebro Delta. Cont. Shelf Res. 74, 94–104. https://doi.org/10.1016/j.csr.2013.11.021.
Liquete, C., Arnau, P., Canals, M., Colas, S., 2005. Mediterranean river systems of Andalusia, southern Spain, and associated deltas: a source to sink approach. Mar. Geol. 222-223, 471–495. https://doi.org/10.1016/j.margeo.2005.06.033.
Liu, J.P., Milliman, J.D., Gao, S., Cheng, P., 2004. Holocene development of the Yellow River's subaqueous delta, North Yellow Sea. Mar. Geol. 209 (1–4), 45–67. https://doi.org/10.1016/j.margeo.2004.06.009.
Liu, J.P., Li, A.C., Xu, K.H., Velozzi, D.M., Yang, Z.S., Milliman, J.D., DeMaster, D.J., 2006. Sedimentary features of the Yangtze River-derived along-shelf clinoform deposit in the East China Sea. Cont. Shelf Res. 26 (17–18 Special Issue in Honor of Richard W. Sternberg's Contributions to Marine Sedimentology), 2141–2156. https://doi.org/10.1016/j.csr.2006.07.013.
Liu, J.P., Xu, K.H., Li, A.C., Milliman, J.D., Velozzi, D.M., Xiao, S.B., Yang, Z.S., 2007. Flux and fate of Yangtze River sediment delivered to the East China Sea. Geomorphology 85 (3–4), 208–224. https://doi.org/10.1016/j.geomorph.2006.03.023.
Liu, J., Saito, Y., Wang, H., Zhou, L., Yang, Z., 2009a. Stratigraphic development during the Late Pleistocene and Holocene offshore of the Yellow River delta, Bohai Sea. J. Asian Earth Sci. 36 (4–5), 318–331. https://doi.org/10.1016/j.jseaes.2009.06.007.
Liu, J.P., Xue, Z., Ross, K., Wang, H.J., Yang, Z.S., Li, A.C., Gao, S., 2009b. Fate of sediments delivered to the sea by Asian large rivers: long-distance transport and formation of remote alongshore clinothems. Sediment. Rec. 7 (4), 4–9.
Liu, J., Kong, X., Saito, Y., Liu, J.P., Yang, Z., Wen, C., 2013. Subaqueous deltaic formation of the Old Yellow River (AD 1128–1855) on the western South Yellow Sea. Mar. Geol. 344, 19–33. https://doi.org/10.1016/j.margeo.2013.07.003.
Liu, J.P., DeMaster, D.J., Nittrouer, C.A., Eidam, E.F., Nguyen, T.T., 2017. A seismic study of the Mekong subaqueous delta: proximal versus distal sediment accumulation. Cont. Shelf Res. 147, 197–212. https://doi.org/10.1016/j.csr.2017.07.009.
Lobo, F.J., Fernández-Salas, L.M., Moreno, I., Sanz, J.L., Maldonado, A., 2006. The sea-floor morphology of a Mediterranean shelf fed by small rivers, northern Alboran Sea margin. Cont. Shelf Res. 26 (20) https://doi.org/10.1016/j.csr.2006.08.006.
Lobo, F.J., Goff, J.A., Mendes, I., Bárcenas, P., Fernández-Salas, L.M., Martín-Rosales, W., Macías, J., Díaz del Río, V., 2015. Spatial variability of prodeltaic undulations on the Guadalfeo River prodelta: support to the genetic interpretation as hyperpycnal flow deposits. Mar. Geophys. Res. 36 (4), 309–333. https://doi.org/10.1007/s11001-014-9233-9.
Maas, G.S., Macklin, M.G., 2002. The impact of recent climate change on flooding and sediment supply within a Mediterranean mountain catchment, southwestern Crete, Greece. Earth Surf. Process. Landf. 27 (10), 1087–1105. https://doi.org/10.1002/esp.398.

Maloney, J.M., Bentley, S.J., Xu, K., Obelcz, J., Georgiou, I.Y., Miner, M.D., 2018. Mississippi River subaqueous delta is entering a stage of retrogradation. Mar. Geol. 400, 12–23. https://doi.org/10.1016/j.margeo.2018.03.001.

Martínez-García, P., Soto, J.I., 2006. Valores de subsidencia reciente (Pioceno-Cuaternario) en el Mar de Alborán mediante análisis de "backstripping". Geogaceta 40, 63–66.

Martín-Puertas, C., Valero-Garcés, B.L., Mata, M.P., González-Sampériz, P., Bao, R., Moreno, A., Stefanova, V., 2008. Arid and humid phases in southern Spain during the last 4000 years: the Zonar Lake record, Cordoba. The Holocene 18 (6), 907–921. https://doi.org/10.1177/0959683608093533.

Maselli, V., Trincardi, F., 2013. Man made deltas. Sci. Rep. 3, 1926. https://doi.org/10.1038/srep01926.

Mendes, I., Lobo, F.J., Fernández-Salas, L.M., López-González, N., Bárcenas, P., Schönfeld, J., Ferreira, Ó., 2015. Multi-proxy evidence of rainfall variability recorded in subaqueous deltaic deposits off the Adra River, Southeast Iberian Peninsula. Estuar. Coast. Shelf Sci. 167 (Part A), 300–312. https://doi.org/10.1016/j.ecss.2015.08.005.

Milli, S., D'Ambrogi, C., Bellotti, P., Calderoni, G., Carboni, M.G., Celant, A., et al., 2013. The transition from wave-dominated estuary to wave-dominated delta: the Late Quaternary stratigraphic architecture of Tiber River deltaic succession (Italy). Sediment. Geol. 284–285 (0), 159–180. https://doi.org/10.1016/j.sedgeo.2012.12.003.

Montojo y Salcedo, J., 1876. Cartas náuticas III. Motril (Granada). Dirección de Hidrografía (Madrid) España.

Moreno, X., Gràcia, E., Bartolomé, R., Martínez-Loriente, S., Perea, H., de la Peña, L.G., Iacono, C. Lo, Piñero, E., Pallàs, R., Masana, E., Dañobeitia, J.J., 2016. Seismostratigraphy and tectonic architecture of the Carboneras Fault offshore based on multiscale seismic imaging: implications for the Neogene evolution of the NE Alboran Sea. Tectonophysics 689, 115–132. https://doi.org/10.1016/j.tecto.2016.02.018.

Moussa, Ben, Tamrouni, O., Hzami, A., Dezileau, L., Mahé, G., Abdeljaouad, S., 2019. Progradation and retrogradation of the Medjerda delta during the 20th century (Tunisia, western Mediterranean). Compt. Rendus Geosci. 351 (4), 340–350. https://doi.org/10.1016/j.crte.2018.10.004.

Navarro-Hervás, F., Ros-Salas, M.-M., Rodríguez-Estrella, T., Fierro-Enrique, E., Carrión, J.-S., García-Veigas, J., Flores, J.-A., Bárcena, M.Á., García, M.S., 2014. Evaporite evidence of a mid-Holocene (c. 4550–4400 cal. yr BP) aridity crisis in southwestern Europe and palaeoenvironmental consequences. The Holocene 24 (4), 489–502. https://doi.org/10.1177/0959683613520260.

Neill, C.F., Allison, M.A., 2005. Subaqueous deltaic formation on the Atchafalaya Shelf, Louisiana. Mar. Geol. 214 (4), 411–430. https://doi.org/10.1016/j.margeo.2004.11.002.

Oguz, T., Mourre, B., Tintoré, J., 2016. Upstream control of the frontal jet regulating plankton production in the Alboran Sea (Western Mediterranean). J. Geophys. Res. Oceans 121 (9), 7159–7175. https://doi.org/10.1002/2016JC011667.

Ortega-Sánchez, M., Lobo, F.J., López-Ruiz, A., Losada, M.A., Fernández-Salas, L.M., 2014. The influence of shelf-indenting canyons and infralittoral prograding wedges on coastal morphology: the Carchuna system in Southern Spain. Mar. Geol. 347 (0), 107–122. https://doi.org/10.1016/j.margeo.2013.11.006.

Palamenghi, L., Schwenk, T., Spiess, V., Kudrass, H.R., 2011. Seismostratigraphic analysis with centennial to decadal time resolution of the sediment sink in the Ganges-Brahmaputra subaqueous delta. Cont. Shelf Res. 31 (6), 712–730. https://doi.org/10.1016/j.csr.2011.01.008.

Pociask-Karteczka, J., 2006. River hydrology and the North Atlantic Oscillation: a general review. AMBIO 35 (6), 312–314. https://doi.org/10.1579/05-S-114.1.

Postma, G., 2001. Physical climate signatures in shallow- and deep-water deltas. Glob. Planet. Chang. 28 (1–4), 93–106. https://doi.org/10.1016/S0921-8181(00)00067-9.

Poulain, P.M., Menna, M., Gerin, R., 2018. Mapping Mediterranean tidal currents with surface drifters. Deep-Sea Res. I Oceanogr. Res. Pap. 138, 22–33. https://doi.org/10.1016/J.DSR.2018.07.011.

Ramos-Román, M.J., Jiménez-Moreno, G., Anderson, R.S., García-Alix, A., Toney, J.L., Jiménez-Espejo, F.J., Carrión, J.S., 2016. Centennial-scale vegetation and North Atlantic Oscillation changes during the Late Holocene in the southern Iberia. Quat. Sci. Rev. 143, 84–95. https://doi.org/10.1016/j.quascirev.2016.05.007.

Rodrigo, F.S., Esteban-Parra, M.J., Pozo-Vázquez, D., Castro-Díez, Y., 2000. Rainfall variability in southern Spain on decadal to centennial time scales. Int. J. Climatol. 20 (7), 721–732. https://doi.org/10.1002/1097-0088(20000615)20:7<721::aid-joc520>3.0.co;2-q.

Sacchi, M., Molisso, F., Violante, C., Esposito, E., Insinga, D., Lubritto, C., et al., 2009. Insights into flood-dominated fan-deltas: Very high-resolution seismic examples off the Amalfi cliffed coasts, eastern Tyrrhenian Sea. In: Violante, C. (Ed.), Geohazard in Rocky Coastal Areas. Geological Society, London, Special Publications, vol. 322. Geological Society, London, pp. 33–71.

Sayol, J.M., Orfila, A., Simarro, G., López, C., Renault, L., Galán, A., Conti, D., 2013. Sea surface transport in the Western Mediterranean Sea: A Lagrangian perspective. J. Geophys. Res. Oceans 118 (12), 6371–6384. https://doi.org/10.1002/2013JC009243.

Slingerland, R., Driscoll, N.W., Milliman, J.D., Miller, S.R., Johnstone, E.A., 2008. Anatomy and growth of a Holocene clinothem in the Gulf of Papua. J. Geophys. Res. Earth Surf. 113 (F01S13) https://doi.org/10.1029/2006JF000628.

Somoza, L., Barnolas, A., Arasa, A., Maestro, A., Rees, J.G., Hernandez-Molina, F.J., 1998. Architectural stacking patterns of the Ebro delta controlled by Holocene high-frequency eustatic fluctuations, delta-lobe switching and subsidence processes. Sediment. Geol. 117 (1–2), 11–32. https://doi.org/10.1016/S0037-0738(97)00121-8.

Stanley, D.J., Warne, A.G., 1994. Worldwide initiation of Holocene Marine Deltas by Deceleration of Sea-Level Rise. Science 265 (5169), 228–231. https://doi.org/10.1126/science.265.5169.228.

Stanley, D.J., Warne, A.G., 1998. Nile Delta in its destruction phase. J. Coast. Res. 14 (3), 795–825. http://www.jstor.org/stable/4298835.

Struglia, M.V., Mariotti, A., Filograsso, A., 2004. River discharge into the Mediterranean Sea: climatology and aspects of the observed variability. J. Clim. 17 (24), 4740–4751. https://doi.org/10.1175/jcli-3225.1.

Syvitski, J., Anthony, E., Saito, Y., Zăinescu, F., Day, J., Bhattacharya, J.P., Giosan, L., 2022. Large deltas, small deltas: toward a more rigorous understanding of coastal marine deltas. Glob. Planet. Chang. 218, 103958 https://doi.org/10.1016/J.GLOPLACHA.2022.103958.

Trincardi, F., Cattaneo, A., Correggiari, A., 2004. Mediterranean prodelta systems. natural evolution and human impact investigated by EURODELTA. Oceanography 17 (4), 34–45. https://doi.org/10.5670/oceanog.2004.02.

Trincardi, F., Amorosi, A., Bosman, A., Correggiari, A., Madricardo, F., Pellegrini, C., 2020. Ephemeral rollover points and clinothem evolution in the modern Po Delta based on repeated bathymetric surveys. Basin Res. 32 (2), 402–418. https://doi.org/10.1111/bre.12426.

Xu, T., Wang, G., Shi, X., Wang, X., Yao, Z., Yang, G., et al., 2016. Sequence stratigraphy of the subaqueous Changjiang (Yangtze River) delta since the Last Glacial Maximum. Sediment. Geol. 331, 132–147. https://doi.org/10.1016/j.sedgeo.2015.10.014.

Xue, Z., Liu, J.P., DeMaster, D., Van Nguyen, L., Ta, T.K.O., 2010. Late Holocene Evolution of the Mekong Subaqueous Delta, Southern Vietnam. Mar. Geol. 269 (1–2), 46–60. https://doi.org/10.1016/j.margeo.2009.12.005.

Yang, S.L., Milliman, J.D., Li, P., Xu, K., 2011. 50,000 dams later: Erosion of the Yangtze River and its delta. Glob. Planet. Chang. 75 (1–2), 14–20. https://doi.org/10.1016/j.gloplacha.2010.09.006.

Yang, H.F., Yang, S.L., Meng, Y., Xu, K.H., Luo, X.X., Wu, C.S., Shi, B.W., 2018. Recent coarsening of sediments on the southern Yangtze subaqueous delta front: a response to river damming. Cont. Shelf Res. 155, 45–51. https://doi.org/10.1016/j.csr.2018.01.012.

Zazo, C., Goy, J.L., Dabrio, C.J., Bardaji, T., Somoza, L., Silva, P.G., 1993. The last interglacial in the Mediterranean as a model for the present interglacial. Glob. Planet. Chang. 7 (1–3), 109–117. https://doi.org/10.1016/0921-8181(93)90043-N.

Zhou, L., Liu, J., Saito, Y., Zhang, Z., Chu, H., Hu, G., 2014. Coastal erosion as a major sediment supplier to continental shelves: example from the abandoned Old Huanghe (Yellow River) delta. Cont. Shelf Res. 82 (0), 43–59. https://doi.org/10.1016/j.csr.2014.03.015.